MULTISCALE MODEL. SIMUL.
Vol. 16, No. 3, pp. 1146–1174

CLOAKING VIA MAPPING FOR THE HEAT EQUATION*

R. V. CRASTER†, S. R. L. GUENNEAU‡, H. R. HUTRIDURGA†, AND G. A. PAVLIOTIS†

Abstract. This paper explores the concept of near-cloaking in the context of time-dependent heat propagation. We show that after the lapse of a certain threshold time, the boundary measurements for the homogeneous heat equation are close to the cloaked heat problem in a certain Sobolev space norm irrespective of the density-conductivity pair in the cloaked region. A regularized transformation media theory is employed to arrive at our results. Our proof relies on the study of the long time behavior of solutions to the parabolic problems with high contrast in density and conductivity coefficients. It further relies on the study of boundary measurement estimates in the presence of small defects in the context of steady conduction problems. We then present some numerical examples to illustrate our theoretical results.

Key words. invisibility cloak, transformation thermodynamics, electric impedance tomography, asymptotic analysis, transformation optics, near-cloaking, parabolic equations

AMS subject classifications. 35K05, 35B40, 35J25, 35R30

DOI. 10.1137/17M1161452

1. Introduction.

1.1. Physical motivation. This work addresses the concept of near-cloaking in the context of time-dependent heat propagation. Our study is motivated by experiments in electrostatics [23] and thermodynamics [37], which have demonstrated the markedly different behavior of structured cloaks in static and dynamic regimes. It has been observed, in the physics literature, that the thermal field in [37] reaches an equilibrium state after a certain time interval, when it looks nearly identical to electrostatic field measured in [23]. There have already been some rigorous results for the electrostatic case [16]. However, during the transient regime the thermal field looks much different from the static result, and a natural question that arises is whether one can give a mathematically rigorous definition of cloaking for diffusion processes in the time domain. This has important practical applications, as cloaking for diffusion processes has been applied to mass transport problems in life sciences [19] and chemistry [38], as well as to multiple light scattering whereby light is governed by ballistic laws [36]. Interestingly, the control of wave trajectories first proposed in the context of electromagnetism [32] can also be extended to matter waves that are solutions of a Schrödinger equation [39] that is akin to the heat equation, and so the near-cloaking we investigate has broad implications and application.

*Received by the editors December 15, 2017; accepted for publication April 13, 2018; published electronically July 17, 2018.
http://www.siam.org/journals/mms/16-3/M116145.html
Funding: The first, second, and third authors' research was supported by the EPSRC programme grant "Mathematical fundamentals of Metamaterials for multiscale Physics and Mechanics" (EP/L024926/1). The first author's research was also supported by the Leverhulme Trust. The fourth author's work was supported by the EPSRC via grants EP/L025159/1, EP/L020564/1, EP/L024926/1, and EP/P031587/1.

†Department of Mathematics, Imperial College London, London, SW7 2AZ, UK (r.craster@imperial.ac.uk, http://www.imperial.ac.uk/people/r.craster; h.hutridurga-ramaiah@imperial.ac.uk, https://hutridurga.wordpress.com; g.pavliotis@imperial.ac.uk, http://www.imperial.ac.uk/people/g.pavliotis).
‡Aix-Marseille Universite, CNRS, Centrale Marseille, Institut Fresnel, 13013, Marseille, France (sebastien.guenneau@fresnel.fr, http://www.fresnel.fr/perso/guenneau/).

1.2. Analytical motivation. Change-of-variables–based cloaking schemes have been inspired by the work of Greenleaf, Lassas, and Uhlmann [16] in the context of electric impedance tomography and by the work of Pendry, Schurig, and Smith [32] in the context of time-harmonic Maxwell's equations. The transformation employed in both those works is singular, and any mathematical analysis involving them becomes quite involved. The transformation in [16, 32] essentially blows up a point to a region in space which needs to be cloaked. These works yield perfect cloaks; i.e., they render the target region completely invisible to boundary measurements. Regularized versions of this singular approach have been proposed in the literature. In [22], Kohn et al. proposed a regularized approximation of this map by blowing up a small ball to a cloaked region and studied the asymptotic behavior as the radius of the small ball vanishes, thus recovering the singular transform of [16, 32]. An alternate approach involving the truncation of singularities was employed by Greenleaf et al. [13] to provide an approximation scheme for the singular transform in [16, 32]. It is to be noted that the constructions in [22, 13] are shown to be equivalent in [20]. We refer the interested reader to the review papers [15, 14] for further details on cloaking via a change-of-variables approach with emphasis on the aforementioned singular transform.

Rather than employing the singular transformation, we follow the lead of Kohn et al. [22], which is in contrast with some works in the literature on the time-dependent thermal cloaking strategies where singular schemes are used; see, e.g., [18, 34, 33]. Note that the evolution equation which we consider is a good model for [37], which designs and fabricates a microstructured thermal cloak that molds the heat flow around an object in a metal plate. We refer the interested reader to the review paper [35] for further details on transformation thermodynamics. The work of Kohn et al. [22] estimates that the near-cloaking they propose for the steady conduction problem is ε^d-close to the perfect cloak, where d is the space dimension. Our construction of the cloaking structure is exactly similar to the construction in [22]. In the present time-dependent setting, we allow the solution to evolve in time until it gets close to the associated thermal equilibrium state which solves a steady conduction problem. This closeness is studied in the Sobolev space $\mathrm{H}^1(\Omega)$. We then employ the ε^d-closeness result of [22] to deduce our near-cloaking theorem in the time-dependent setting. To the best of our knowledge, this is the first work to consider near-cloaking strategies to address the time-dependent heat conduction problem.

In the literature, there have been numerous works on the approximate cloaking strategies for the Helmholtz equation [21, 24, 26, 25] (see also [27] for the treatment of the full wave equation). The strategy in [27] to treat the time-dependent wave problem is to take the Fourier transform in the time variable. This yields a family of Helmholtz problems (family indexed by the frequency). The essential idea there is to obtain appropriate degree of invisibility estimates for the Helmholtz equation—the estimates being frequency-dependent. More importantly, these estimates blow up in the frequency regime. But, they do so in an integrable fashion. Equipped with these approximate cloaking results for the Helmholtz equations, the authors in [27] simply invert the Fourier transform to read off the near-cloaking result for the time-dependent wave equation. Inspired by [27], one could apply the Laplace transform in the time variable for the heat equation and try to mimic the analysis in [27] for the family of elliptic problems thus obtained. Note that this approach does not require, unlike ours, the solution to the heat conduction problem to reach equilibrium state to obtain approximate cloaking. We have not explored this approach in detail and we leave it for future investigations.

Gralak et al. [12] recently developed invisible layered structures in transforma-

tion optics in the temporal regime. Inspired by that work, we have also developed a transformation media theory for thermal layered cloaks, which are of practical importance in thin-film solar cells for energy harvesting in the photovoltaic industry. These layered cloaks might be of importance in thermal imaging. We direct the interested reader to [3] and references therein.

In the applied mathematics community working on metamaterials, enhancement of near-cloaking is another topic which has been addressed in the literature. Loosely speaking, these enhancement techniques involve covering a small ball of radius ε by multiple coatings and then applying the push-forward maps of [22]. These multiple coatings which result in the vanishing of certain polarization tensors help us improve the ε^d-closeness of [22] to ε^{dN}-closeness, where N denotes the number of coatings in the above construction. For further details, we direct the reader to [7, 6] in the mathematics literature and [1, 2] in the physics literature (the works [1, 2] employ negative index materials). One could employ the constructions of [7, 6] in the time-independent setting to our temporal setting to obtain enhanced near-cloaking structures. This again is left for future investigations.

In this present work, we are able to treat time-independent sources for the heat equation. As our approach involves the study of thermal equilibration, we could extend our result to time-dependent sources which result in equilibration. This, however, leaves open the question of near-cloaking for the heat equation with genuinely time-dependent sources which do not result in thermal equilibration. For example, sources which are time harmonic cannot be treated by the approach of this paper. The approach involving the Laplace transform mentioned in a previous paragraph might be of help here. There are plenty of numerical works published by physicists on these aspects but with no mathematical foundation thus far. The authors plan to return to these questions in the near future.

1.3. Paper structure. The paper is organized as follows. In section 2, we briefly recall the change-of-variable-principle for the heat equation. This section also makes precise the notion of near-cloaking and its connection to perfect cloaking followed by the construction of cloaking density and conductivity coefficients. Our main result (Theorem 2) is stated in that section. Section 3 deals with the long time behavior of solutions to parabolic problems; the effect of high contrast in density and conduction on the long time behavior of solutions is also treated in that section. The proof of Theorem 2 is given in section 4. In this section, we also develop upon an idea of layered cloak inspired by the construction in [12]. Finally, in section 5, we present some numerical examples to illustrate our theoretical results.

2. Mathematical setting. Let $\Omega \subset \mathbb{R}^d$ $(d = 2, 3)$ be a smooth bounded domain such that $B_2 \subset \Omega$. Throughout, we use the notation B_r to denote a euclidean ball of radius r centered at the origin.

2.1. Change-of-variables principle. The following result recalls the principle behind the change-of-variables–based cloaking strategies. This is the typical, and essential, ingredient of any cloaking strategy in transformation media theory.

PROPOSITION 1. *Let the coefficients $A \in \mathrm{L}^\infty(\Omega; \mathbb{R}^{d\times d})$ and $\rho \in \mathrm{L}^\infty(\Omega; \mathbb{R})$. Suppose the source term $f \in \mathrm{L}^2(\Omega; \mathbb{R})$. Consider a smooth invertible map $\mathbb{F} : \Omega \mapsto \Omega$ such that $\mathbb{F}(x) = x$ for each $x \in \Omega \setminus B_2$. Furthermore, assume that the associated Jacobians satisfy $\det(D\mathbb{F})(x), \det(D\mathbb{F}^{-1})(x) \geq C > 0$ for a.e. $x \in \Omega$. Then $u(t, x)$ is a solution to*

$$\rho(x)\frac{\partial u}{\partial t} = \nabla \cdot \Big(A(x)\nabla u\Big) + f(x) \qquad \text{for } (t, x) \in (0, \infty) \times \Omega$$

if and only if $v = u \circ \mathbb{F}^{-1}$ *is a solution to*

$$\mathbb{F}^*\rho(y)\frac{\partial v}{\partial t} = \nabla \cdot \Big(\mathbb{F}^* A(y)\nabla v\Big) + \mathbb{F}^* f(y) \qquad \text{for } (t,y) \in (0,\infty)\times\Omega,$$

where the coefficients are given as

$$\begin{aligned} \mathbb{F}^*\rho(y) &= \frac{\rho(x)}{\det(D\mathbb{F})(x)}; & \mathbb{F}^* f(t,y) &= \frac{f(t,x)}{\det(D\mathbb{F})(x)}; \\ \mathbb{F}^* A(y) &= \frac{D\mathbb{F}(x)A(x)D\mathbb{F}^\top(x)}{\det(D\mathbb{F})(x)} \end{aligned} \tag{2.1}$$

with the understanding that the right-hand sides in (2.1) *are computed at* $x = \mathbb{F}^{-1}(y)$. *Moreover, we have for all* $t > 0$,

$$u(t,\cdot) = v(t,\cdot) \qquad \text{in } \Omega \setminus B_2. \tag{2.2}$$

The proof of the above proposition has appeared in the literature in most of the papers on "cloaking via mapping" techniques. It essentially involves performing a change of variables in the weak formulation associated with the differential equation. We will skip the proof and refer the reader to [22, subsection 2.2], [21, subsection 2.2, page 976], [18, section 2, page 8209] for essential details.

Following Kohn et al. [22], we fix a regularizing parameter $\varepsilon > 0$ and consider a Lipschitz map $\mathcal{F}_\varepsilon : \Omega \mapsto \Omega$ defined below:

$$\mathcal{F}_\varepsilon(x) := \begin{cases} x & \text{for } x \in \Omega \setminus B_2, \\ \left(\frac{2-2\varepsilon}{2-\varepsilon} + \frac{|x|}{2-\varepsilon}\right)\frac{x}{|x|} & \text{for } x \in B_2 \setminus B_\varepsilon, \\ \frac{x}{\varepsilon} & \text{for } x \in B_\varepsilon. \end{cases} \tag{2.3}$$

Note that $\mathcal{F}_\varepsilon$ maps B_ε to B_1 and the annulus $B_2 \setminus B_\varepsilon$ to $B_2 \setminus B_1$. The cloaking strategy with the above map corresponds to having B_1 as the cloaked region and the annulus $B_2 \setminus B_1$ as the cloaking annulus. The Lipschitz map given above is borrowed from [22, page 5]. Remark that taking $\varepsilon = 0$ in (2.3) yields the map

$$\mathcal{F}_0(x) := \begin{cases} x & \text{for } x \in \Omega \setminus B_2, \\ \left(1 + \frac{1}{2}|x|\right)\frac{x}{|x|} & \text{for } x \in B_2 \setminus \{0\}, \end{cases} \tag{2.4}$$

which is the singular transform of [16, 32]. The map $\mathcal{F}_0$ is smooth except at the point 0. It maps 0 to B_1 and $B_2 \setminus \{0\}$ to $B_2 \setminus B_1$.

2.2. Essential idea of the paper. Let us make precise the notion of near-cloaking we will use throughout this paper. Let $f \in \mathrm{L}^2(\Omega)$ denote a source term such that $\operatorname{supp} f \subset \Omega \setminus B_2$. Let $g \in \mathrm{L}^2(\partial\Omega)$ denote a Neumann boundary datum. Suppose the initial datum $u^{\mathrm{in}} \in \mathrm{H}^1(\Omega)$ is such that $\operatorname{supp} u^{\mathrm{in}} \subset \Omega \setminus B_2$. Consider the homogeneous (conductivity being unity) heat equation for the unknown $u_{\mathrm{hom}}(t,x)$ with the aforementioned data:

$$\begin{aligned} \partial_t u_{\mathrm{hom}}(t,x) &= \Delta u_{\mathrm{hom}}(t,x) + f(x) && \text{in } (0,\infty)\times\Omega, \\ \nabla u_{\mathrm{hom}} \cdot \mathbf{n}(x) &= g(x) && \text{on } (0,\infty)\times\partial\Omega, \\ u_{\mathrm{hom}}(0,x) &= u^{\mathrm{in}}(x) && \text{in } \Omega. \end{aligned} \tag{2.5}$$

Here $\mathbf{n}(x)$ is the unit exterior normal to Ω at $x \in \partial\Omega$.

Our objective is to construct coefficients $\rho_{\rm cl}(x)$ and $A_{\rm cl}(x)$ such that

$$\rho_{\rm cl}(x) = \eta(x); \qquad A_{\rm cl}(x) = \beta(x) \qquad \text{in } B_1$$

for some arbitrary bounded positive density η and for some arbitrary bounded positive definite conductivity β. This construction should further imply that the evolution for the unknown $u_{\rm cl}(t,x)$ given by

$$\begin{aligned} \rho_{\rm cl}(x)\partial_t u_{\rm cl} &= \nabla \cdot \Big(A_{\rm cl}(x) \nabla u_{\rm cl} \Big) + f(x) && \text{in } (0,\infty)\times\Omega, \\ \nabla u_{\rm cl} \cdot \mathbf{n}(x) &= g(x) && \text{on } (0,\infty)\times\partial\Omega, \\ u_{\rm cl}(0,x) &= u^{\rm in}(x) && \text{in } \Omega \end{aligned} \tag{2.6}$$

is such that there exists a time instant $T < \infty$ so that for all $t \geq T$, we have

$$u_{\rm cl}(t,x) \approx u_{\rm hom}(t,x) \qquad \text{for } x \in \Omega \setminus B_2.$$

The above closeness will be measured in some appropriate function space norm. Most importantly, this approximation should be independent of the density-conductivity pair η, β in B_1. Note, in particular, that the source terms $f(x), g(x), u^{\rm in}(x)$ in (2.5) and (2.6) are the same.

2.3. Cloaking coefficients and the defect problem. The following construct using the push-forward maps is now classical in transformation optics, and we use it here for thermodynamics:

$$\rho_{\rm cl}(x) = \begin{cases} 1 & \text{for } x \in \Omega \setminus B_2, \\ \mathcal{F}_\varepsilon^* 1 & \text{for } x \in B_2 \setminus B_1, \\ \eta(x) & \text{for } x \in B_1 \end{cases} \tag{2.7}$$

and

$$A_{\rm cl}(x) = \begin{cases} \mathrm{Id} & \text{for } x \in \Omega \setminus B_2, \\ \mathcal{F}_\varepsilon^* \mathrm{Id} & \text{for } x \in B_2 \setminus B_1, \\ \beta(x) & \text{for } x \in B_1. \end{cases} \tag{2.8}$$

The density coefficient $\eta(x)$ in (2.7) is any arbitrary real coefficient such that

$$0 < \eta(x) < \infty \qquad \text{for } x \in B_1.$$

The conductivity coefficient $\beta(x)$ in (2.8) is any arbitrary bounded positive definite matrix; i.e., there exist positive constants κ_1 and κ_2 such that

$$\kappa_1 |\xi|^2 \leq \beta(x)\xi \cdot \xi \leq \kappa_2 |\xi|^2 \qquad \forall (x,\xi) \in B_1 \times \mathbb{R}^d.$$

The following observation is crucial for the analysis to follow. Consider the density-conductivity pair

$$\rho^\varepsilon(x) = \begin{cases} 1 & \text{for } x \in \Omega \setminus B_\varepsilon, \\ \frac{1}{\varepsilon^d}\eta\left(\frac{x}{\varepsilon}\right) & \text{for } x \in B_\varepsilon \end{cases} \tag{2.9}$$

and

$$A^\varepsilon(x) = \begin{cases} \mathrm{Id} & \text{for } x \in \Omega \setminus B_\varepsilon, \\ \frac{1}{\varepsilon^{d-2}} \beta\left(\frac{x}{\varepsilon}\right) & \text{for } x \in B_\varepsilon. \end{cases} \tag{2.10}$$

Next, let us compute their push-forwards using the Lipschitz map $\mathcal{F}^\varepsilon$—as given by the formulae (2.1)—yielding

$$\rho_{\mathrm{cl}}(y) = \mathcal{F}^*_\varepsilon \rho^\varepsilon(y); \qquad A_{\mathrm{cl}}(y) = \mathcal{F}^*_\varepsilon A^\varepsilon(y).$$

Then the assertion of Proposition 1 (see, in particular, the equality (2.2)) implies that the solution $u_{\mathrm{cl}}(t,x)$ to (2.6) satisfies for all $t > 0$,

$$u_{\mathrm{cl}}(t,x) = u^\varepsilon(t,x) \qquad \forall x \in \Omega \setminus B_2$$

with $u^\varepsilon(t,x)$ being the solution to

$$\begin{aligned} \rho^\varepsilon(x)\partial_t u^\varepsilon &= \nabla \cdot \left(A^\varepsilon(x)\nabla u^\varepsilon\right) + f(x) && \text{in } (0,\infty)\times\Omega, \\ \nabla u^\varepsilon \cdot \mathbf{n}(x) &= g(x) && \text{on } (0,\infty)\times\partial\Omega, \\ u^\varepsilon(0,x) &= u^{\mathrm{in}}(x) && \text{in } \Omega \end{aligned} \tag{2.11}$$

with the coefficients in the above evolution being given by (2.9)–(2.10). The coefficients ρ^ε and A^ε are uniform except for their values in B_ε. Hence we treat B_ε as a defect where the coefficients show high contrast with respect to their values elsewhere in the domain. Due to the nature of these coefficients, we call the evolution problem (2.11) the *defect problem with high contrast coefficients* or *defect problem* for short. The change-of-variables principle (see Proposition 1) essentially says that, to study cloaking for the transient heat transfer problem, we need to compare the solution $u^\varepsilon(t,x)$ to the defect problem (2.11) with the solution $u_{\mathrm{hom}}(t,x)$ to the homogeneous problem (2.5) for $x \in \Omega \setminus B_2$.

2.4. Main result. We are now ready to state the main result of this work.

THEOREM 2. *Let the dimension $d \geq 2$. Let $u^\varepsilon(t,x)$ be the solution to the defect problem* (2.11)*, and let $u_{\mathrm{hom}}(t,x)$ be the solution to the homogeneous conductivity problem* (2.5)*. Suppose the data in* (2.5) *and* (2.11) *are such that*

$$f \in \mathrm{L}^2(\Omega), \quad \operatorname{supp} f \subset \Omega \setminus B_2, \quad g \in \mathrm{L}^2(\partial\Omega), \quad u^{\mathrm{in}} \in \mathrm{H}^1(\Omega), \quad \operatorname{supp} u^{\mathrm{in}} \subset \Omega \setminus B_2.$$

Let us further suppose that the source terms satisfy

$$\int_\Omega f(x)\,\mathrm{d}x + \int_{\partial\Omega} g(x)\,\mathrm{d}\sigma(x) = 0, \tag{2.12}$$

$$\int_\Omega u^{\mathrm{in}}(x)\,\mathrm{d}x = 0. \tag{2.13}$$

Then there exists a time $T < \infty$ such that for all $t \geq T$, we have

$$\|u^\varepsilon(t,\cdot) - u_{\mathrm{hom}}(t,\cdot)\|_{\mathrm{H}^{\frac{1}{2}}(\partial\Omega)} \leq C\left(\left\|u^{\mathrm{in}}\right\|_{\mathrm{H}^1} + \|f\|_{\mathrm{L}^2(\Omega)} + \|g\|_{\mathrm{L}^2(\partial\Omega)}\right)\varepsilon^d, \tag{2.14}$$

where the positive constant C depends on the domain Ω and the L^∞ bounds on the density-conductivity pair (η,β) in B_1.

Thanks to the change-of-variables principle (Proposition 1), we deduce the following corollary.

COROLLARY 3. *Let $u_{\mathrm{cl}}(t,x)$ be the solution to the thermal cloak problem* (2.6) *with the cloaking coefficients $\rho_{\mathrm{cl}}(x), A_{\mathrm{cl}}(x)$ given by* (2.7)–(2.8). *Let $u_{\mathrm{hom}}(t,x)$ be the solution to the homogeneous conductivity problem* (2.5). *Suppose the data in* (2.5) *and* (2.6) *are such that*

$$f \in \mathrm{L}^2(\Omega), \quad \operatorname{supp} f \subset \Omega \setminus B_2, \quad g \in \mathrm{L}^2(\partial\Omega), \quad u^{\mathrm{in}} \in \mathrm{H}^1(\Omega), \quad \operatorname{supp} u^{\mathrm{in}} \subset \Omega \setminus B_2.$$

Let us further suppose that the source terms satisfy (2.12) *and* (2.13). *Then there exists a time $T < \infty$ such that for all $t \geq T$, we have*

$$\|u_{\mathrm{cl}}(t,\cdot) - u_{\mathrm{hom}}(t,\cdot)\|_{\mathrm{H}^{\frac{1}{2}}(\partial\Omega)} \leq C\left(\left\|u^{\mathrm{in}}\right\|_{\mathrm{H}^1} + \|f\|_{\mathrm{L}^2(\Omega)} + \|g\|_{\mathrm{L}^2(\partial\Omega)}\right)\varepsilon^d, \tag{2.15}$$

where the positive constant C depends on the domain Ω and the L^∞ bounds on the density-conductivity pair (η,β) in B_1.

Whenever the source terms $f(x), g(x)$ and the initial datum $u^{\mathrm{in}}(x)$ satisfy the compatibility conditions (2.12)–(2.13), we shall call them *admissible*. Our proof of the Theorem 2 relies upon two ideas:

(i) long time behavior of solutions to parabolic problems and
(ii) boundary measurement estimates in the presence of small inhomogeneities.

Remark 4. Our strategy of proof goes via the study of the steady-state problems associated with the evolutions (2.5) and (2.11). Those elliptic boundary value problems demand that the source terms be compatible to guarantee existence and uniqueness of solution. These compatibility conditions on the bulk and Neumann boundary sources f, g translate to the zero mean assumption (2.12). Note that the compatibility condition (2.12) is not necessary for the well-posedness of the transient problems.

Remark 5. Ammari et al. [3] have proved a result that is closely related to our near-cloaking result (Theorem 2). Our main result says that near-cloaking for the heat equation is possible once the system is driven close to its equilibrium state, and thus it can be interpreted as a large time asymptotic result. The result in [3], however, can be interpreted as a short time near-cloaking result. They prove that the solution $u^\varepsilon(t,x)$ to the small defect problem (2.11) and the solution $u_{\mathrm{hom}}(t,x)$ to the homogeneous conductivity problem (2.5) are close to each other (see [3, Lemma 3.2, page 1120]) as follows:

$$\sup_{0\leq t\leq T} \|u^\varepsilon(t,\cdot) - u_{\mathrm{hom}}(t,\cdot)\|_{\mathrm{L}^2(\Omega)} + \|\nabla u^\varepsilon(t,\cdot) - \nabla u_{\mathrm{hom}}(t,\cdot)\|_{\mathrm{L}^2((0,T)\times\Omega)} \leq C\sqrt{T}\varepsilon^{\frac{d}{2}}.$$

Note that in the above estimate, the larger the time instant T, the worse the estimate gets. Also, the results in [3] are carried out for an isotropic background with isotropic inclusions. But, their proof carries over to our setting of anisotropic inclusion as well. The authors of [3] derive first-order small volume expansion with precise estimates on the remainder (see [3, Theorem 2.1, page 1118]).

A remark about the assumption (2.13) on the initial datum u^{in} in Theorem 2 will be made after the proof of Theorem 2, as it will be clearer to the reader.

3. Study of the long time behavior. In this section, we deal with the long time asymptotic analysis for the parabolic problems. Consider the initial-boundary value problem for the unknown $v(t,x)$:

$$\begin{aligned} \partial_t v &= \Delta v && \text{in } (0,\infty)\times\Omega, \\ \nabla v\cdot\mathbf{n}(x) &= 0 && \text{on } (0,\infty)\times\partial\Omega, \\ v(0,x) &= v^{\text{in}}(x) && \text{in } \Omega. \end{aligned} \tag{3.1}$$

We give an asymptotic result for the solution to (3.1) in the $t\to\infty$ limit.

PROPOSITION 6. *Let $v(t,x)$ be the solution to the initial-boundary value problem (3.1). Suppose we have the initial datum $v^{\text{in}}\in \mathrm{H}^1(\Omega)$. Then there exists a constant $\gamma>0$ such that*

$$\left\|v(t,\cdot)-\langle v^{\text{in}}\rangle\right\|_{\mathrm{H}^1(\Omega)} \le e^{-\gamma t}\left\|v^{\text{in}}\right\|_{\mathrm{H}^1(\Omega)} \qquad \text{for all } t>0, \tag{3.2}$$

where $\langle v^{\text{in}}\rangle$ denotes the initial average, i.e.,

$$\langle v^{\text{in}}\rangle := \frac{1}{|\Omega|}\int_\Omega v^{\text{in}}(x)\,\mathrm{d}x.$$

Proof of the above proposition is standard and is based on the spectral study of the corresponding elliptic problem; see, e.g., [31]. Alternatively, we could also use energy methods based on a priori estimates on the solution of the parabolic partial differential equations; see, e.g., [10, Chapter 13]. As the proof of Proposition 6 is quite standard, we omit the proof.

Let us recall certain notions necessary for our proof. Let $\{\varphi_k\}_{k=1}^\infty\subset \mathrm{H}^1(\Omega)$ denote the collection of Neumann Laplacian eigenfunctions on Ω, i.e., for each $k\in\mathbb{N}$,

$$\begin{aligned} -\Delta\varphi_k &= \mu_k\varphi_k && \text{in } \Omega, \\ \nabla\varphi_k\cdot\mathbf{n}(x) &= 0 && \text{on } \partial\Omega, \end{aligned} \tag{3.3}$$

with $\{\mu_k\}$ denoting the eigenvalues. Recall that the spectrum is discrete, nonnegative, and with no finite accumulation point, i.e.,

$$0=\mu_1\le\mu_2\le\cdots\to\infty.$$

The next proposition is a result similar in flavor to Proposition 6 but in a more general parabolic setting with high contrast in density and conductivity coefficients. More precisely, let us consider the heat equation with uniform conductivity in the presence of a defect with high contrast coefficients. We particularly choose the conductivity matrix to be (2.10) and the density coefficient to be (2.9). For an unknown $v^\varepsilon(t,x)$, consider the initial-boundary value problem

$$\begin{aligned} \rho^\varepsilon(x)\partial_t v^\varepsilon &= \nabla\cdot\left(A^\varepsilon(x)\nabla v^\varepsilon\right) && \text{in } (0,\infty)\times\Omega, \\ \nabla v^\varepsilon\cdot\mathbf{n}(x) &= 0 && \text{on } (0,\infty)\times\partial\Omega, \\ v^\varepsilon(0,x) &= v^{\text{in}}(x) && \text{in } \Omega. \end{aligned} \tag{3.4}$$

We give an asymptotic result for the solution $v^\varepsilon(t,x)$ to (3.4) in the $t\to\infty$ limit. As before, we are interested in the $\|\cdot\|_{\mathrm{H}^1}$-norm rather than the $\|\cdot\|_{\mathrm{L}^2}$-norm.

PROPOSITION 7. *Let $v^\varepsilon(t,x)$ be the solution to the initial-boundary value problem (3.4). Suppose we have the initial datum $v^{\text{in}} \in \mathrm{H}^1(\Omega) \cap \mathrm{L}^\infty(\Omega)$. Then there exists a constant $\gamma_\varepsilon > 0$ such that for all $t > 0$, we have*

$$\|v^\varepsilon(t,\cdot) - \mathfrak{m}^\varepsilon\|_{\mathrm{H}^1(\Omega)} \leq e^{-\gamma_\varepsilon t}\left(\frac{1}{\varepsilon^d}\left\|v^{\text{in}}\right\|_{\mathrm{L}^2(\Omega)} + \frac{1}{\varepsilon^{\frac{d-2}{2}}}\left\|\nabla v^{\text{in}}\right\|_{\mathrm{L}^2(\Omega)}\right), \tag{3.5}$$

where $\mathfrak{m}^\varepsilon$ denotes the following weighted initial average:

$$\mathfrak{m}^\varepsilon := \frac{1}{|\Omega|\,\langle\rho^\varepsilon\rangle}\int_\Omega \rho^\varepsilon(x)v^{\text{in}}(x)\,\mathrm{d}x \qquad \textit{with} \quad \langle\rho^\varepsilon\rangle = \frac{1}{|\Omega|}\int_\Omega \rho^\varepsilon(x)\,\mathrm{d}x.$$

Remark 8. From estimate (3.5) we conclude that the estimate on the right-hand side is a product of an exponential decay term and a term of $\mathcal{O}(\varepsilon^{-d})$. So, if $\gamma^\varepsilon \gtrsim 1$, uniformly in ε, then the solution converges to the weighted initial average in the long time regime. We will demonstrate that the decay rate γ^ε is bounded away from zero uniformly (with respect to ε) in subsection 3.1.

If the density coefficient $\rho^\varepsilon(x)$ is given by (2.9), then

$$\langle\rho^\varepsilon\rangle = \frac{1}{|\Omega|}\left\{\int_{\Omega\setminus B_\varepsilon} 1\,\mathrm{d}x + \frac{1}{\varepsilon^d}\int_{B_\varepsilon} 1\,\mathrm{d}x\right\} = \frac{1}{|\Omega|}\left(|\Omega\setminus B_\varepsilon| + \frac{\pi^{\frac{d}{2}}}{\Gamma\left(\frac{d}{2}+1\right)}\right),$$

where $\Gamma(\cdot)$ denotes the gamma function. Substituting for $\langle\rho^\varepsilon\rangle$ in the expression for the weighted initial average yields

$$\mathfrak{m}^\varepsilon = \left(|\Omega\setminus B_\varepsilon| + \frac{\pi^{\frac{d}{2}}}{\Gamma\left(\frac{d}{2}+1\right)}\right)^{-1}\left\{\int_{\Omega\setminus B_\varepsilon} v^{\text{in}}(x)\,\mathrm{d}x + \frac{1}{\varepsilon^d}\int_{B_\varepsilon} v^{\text{in}}(x)\,\mathrm{d}x\right\}.$$

Using the assumption on the initial datum v^{in} that it belongs to $\mathrm{H}^1(\Omega)\cap\mathrm{L}^\infty(\Omega)$, we get the following uniform bound (uniform with respect to ε) on the weighted initial average:

$$|\mathfrak{m}^\varepsilon| \leq 1 + \frac{|\Omega|\,\Gamma\left(\frac{d}{2}+1\right)}{\pi^{\frac{d}{2}}}\left\|v^{\text{in}}\right\|_{\mathrm{L}^2(\Omega)} < \infty.$$

Proof of Proposition 7. Let μ_k^ε and φ_k^ε be the Neumann eigenvalues and eigenfunctions defined as

$$\begin{aligned} -\nabla\cdot\left(A^\varepsilon\nabla\varphi_k^\varepsilon\right) &= \mu_k^\varepsilon\rho^\varepsilon\varphi_k^\varepsilon \qquad \text{in } \Omega,\\ \nabla\varphi_k^\varepsilon\cdot\mathbf{n}(x) &= 0 \qquad\qquad\quad \text{on } \partial\Omega, \end{aligned} \tag{3.6}$$

where the conductivity-density pair $A^\varepsilon(x)$, $\rho^\varepsilon(x)$ is given by (2.10)–(2.9). Here again the spectrum is discrete, nonnegative, and with no finite accumulation point, i.e.,

$$0 = \mu_1^\varepsilon \leq \mu_2^\varepsilon \leq \cdots \to \infty.$$

The solution $v^\varepsilon(t,x)$ to (3.4) can be represented in terms of the basis functions $\{\varphi_k^\varepsilon\}_{k=1}^\infty$ as

$$v^\varepsilon(t,x) = \sum_{k=1}^\infty \mathfrak{b}_k^\varepsilon(t)\varphi_k^\varepsilon(x) \qquad \text{with} \quad \mathfrak{b}_k^\varepsilon(t) = \int_\Omega v^\varepsilon(t,x)\rho^\varepsilon(x)\varphi_k^\varepsilon(x)\,\mathrm{d}x.$$

The general representation formula for the solution to (3.4) becomes

$$v^\varepsilon(t,x) = \sum_{k=1}^{\infty} \mathfrak{b}_k^\varepsilon(0) e^{-\mu_k t}\varphi_k(x) = \mathfrak{b}_1^\varepsilon(0)\varphi_1^\varepsilon + \sum_{k=2}^{\infty} \mathfrak{b}_k^\varepsilon(0) e^{-\mu_k^\varepsilon t}\varphi_k^\varepsilon(x). \tag{3.7}$$

The first term in the above representation is nothing but the weighted initial average

$$\varphi_1^\varepsilon \mathfrak{b}_1^\varepsilon(0) = |\varphi_1^\varepsilon|^2 \int_\Omega v^{\mathrm{in}}(x)\rho^\varepsilon(x)\,\mathrm{d}x = \frac{1}{|\Omega|\,\langle \rho^\varepsilon\rangle}\int_\Omega v^{\mathrm{in}}(x)\rho^\varepsilon(x)\,\mathrm{d}x =: \mathfrak{m}^\varepsilon.$$

The representation (3.7) says that the weighted $\mathrm{L}^2(\Omega)$-norm of $v^\varepsilon(t,x)$ is

$$\|v^\varepsilon(t,\cdot)\|^2_{\mathrm{L}^2(\Omega;\rho^\varepsilon)} = |\mathfrak{b}_1^\varepsilon(0)|^2 + \sum_{k=2}^{\infty} |\mathfrak{b}_k^\varepsilon(0)|^2\, e^{-2\mu_k^\varepsilon t},$$

where we have used the following notation for the weighted Lebesgue space norm:

$$\|w\|_{\mathrm{L}^2(\Omega;\rho^\varepsilon)} := \int_\Omega w(x)\rho^\varepsilon(x)\,\mathrm{d}x.$$

The density coefficient $\rho^\varepsilon(x)$ defined in (2.9) appears as the weight function in the above Lebesgue space. It follows that

$$\|w\|_{\mathrm{L}^2(\Omega)} \lesssim \|w\|_{\mathrm{L}^2(\Omega;\rho^\varepsilon)} \lesssim \frac{1}{\varepsilon^d}\,\|w\|_{\mathrm{L}^2(\Omega)}$$

thanks to the definition of $\rho^\varepsilon(x)$ in (2.9). Computing the weighted norm of the difference $v^\varepsilon(t,x) - \mathfrak{m}^\varepsilon$, we get

$$\|v^\varepsilon(t,\cdot) - \mathfrak{m}^\varepsilon\|^2_{\mathrm{L}^2(\Omega;\rho^\varepsilon)} = \sum_{k=2}^{\infty} |\mathfrak{b}_k^\varepsilon(0)|^2\, e^{-2\mu_k^\varepsilon t} \le e^{-2\mu_2^\varepsilon t}\left\|v^{\mathrm{in}}\right\|^2_{\mathrm{L}^2(\Omega;\rho^\varepsilon)}.$$

Hence we deduce that

$$\|v^\varepsilon(t,\cdot) - \mathfrak{m}^\varepsilon\|^2_{\mathrm{L}^2(\Omega)} \le e^{-2\mu_2^\varepsilon t}\frac{1}{\varepsilon^{2d}}\left\|v^{\mathrm{in}}\right\|^2_{\mathrm{L}^2(\Omega)}. \tag{3.8}$$

Next, it follows from the representation formula (3.7) that

$$\sqrt{A^\varepsilon(x)}\nabla v^\varepsilon(t,x) = \sum_{k=2}^{\infty} \mathfrak{b}_k^\varepsilon(0) e^{-\mu_k^\varepsilon t}\sqrt{A^\varepsilon(x)}\nabla\varphi_k^\varepsilon(x),$$

which in turn implies that

$$\begin{aligned}\left\|\sqrt{A^\varepsilon}\nabla v^\varepsilon\right\|^2_{\mathrm{L}^2(\Omega)} &= \sum_{k=2}^{\infty} |\mathfrak{b}_k^\varepsilon(0)|^2\,\mu_k^\varepsilon\, e^{-2\mu_k^\varepsilon t} \le e^{-2\mu_2^\varepsilon t}\sum_{k=2}^{\infty} |\mathfrak{b}_k^\varepsilon(0)|^2\,\mu_k^\varepsilon \\ &= e^{-2\mu_2^\varepsilon t}\left\|\sqrt{A^\varepsilon}\nabla v^{\mathrm{in}}\right\|^2_{\mathrm{L}^2(\Omega)} \le e^{-2\mu_2^\varepsilon t}\frac{1}{\varepsilon^{d-2}}\left\|\nabla v^{\mathrm{in}}\right\|^2_{\mathrm{L}^2(\Omega)}.\end{aligned}$$

Furthermore, as $1 \lesssim \|A^\varepsilon\|_{\mathrm{L}^\infty}$, it follows that

$$\|\nabla v^\varepsilon\|^2_{\mathrm{L}^2(\Omega)} \le e^{-2\mu_2^\varepsilon t}\frac{1}{\varepsilon^{d-2}}\left\|\nabla v^{\mathrm{in}}\right\|^2_{\mathrm{L}^2(\Omega)}.$$

Repeating the above computations for the difference $v^\varepsilon(t,x) - \mathfrak{m}^\varepsilon$, we obtain

$$\|\nabla\left(v^\varepsilon - \mathfrak{m}^\varepsilon\right)\|^2_{\mathrm{L}^2(\Omega)} \leq e^{-2\mu_2^\varepsilon t}\frac{1}{\varepsilon^{d-2}}\left\|\nabla v^{\mathrm{in}}\right\|^2_{\mathrm{L}^2(\Omega)}. \tag{3.9}$$

Gathering the inequalities (3.8)–(3.9) together proves the proposition with the constant $\gamma_\varepsilon = \mu_2^\varepsilon$, i.e., the first nonzero Neumann eigenvalue in the spectral problem (3.6) on Ω with the high contrast density-conductivity pair $(\rho^\varepsilon(x), A^\varepsilon(x))$. ∎

3.1. Reduction to a Schrödinger operator. The constants γ and γ^ε in Propositions 6 and 7, respectively, give the rate of convergence to equilibrium. As the proofs in the previous subsection suggest, these rates are nothing but the first nonzero eigenvalues of the associated Neumann eigenvalue problems.

The constant decay rate γ_ε in Proposition 7 may depend on the regularization parameter ε. In our setting, ε is nothing but the radius of the inclusion. Hence, to understand the behavior of γ^ε in terms of ε, we need to study the perturbations in the eigenvalues caused by the presence of inhomogeneities with conductivities and densities different from the background conductivity and density. More importantly, we need to understand the spectrum of transmission problems with high contrast conductivities and densities. The spectral analysis of elliptic operators with such conductivity matrices is done extensively in the literature in the context of electric impedance tomography; see [8, 5] and references therein for further details. In [8], for example, the authors give an asymptotic expansion for the eigenvalues μ_k^ε in terms of the regularizing parameter ε (even in the case of multiplicities). We refer the reader to [8, equation (23), page 74] for the precise expansion. For high contrast conductivities such as A^ε, we refer the reader to the concluding remarks in [8, pages 74–75] and references therein. Another important point to be noted is that the above mentioned works of Ammari and co-authors do not treat high contrast densities while addressing the spectral problems. For our setting—more specifically for the spectral problem (3.6)—the reader is directed to consult the review paper of Chechkin [9], which goes into detail about the spectral problem in a related setting. Furthermore, the review paper [9] gives exhaustive reference to literature where similar spectral problems are addressed.

Rather than deducing the behavior of the first nonzero eigenvalue of the spectral problem (3.6) from [9], we propose an alternate approach. Studying (3.6) is the same as the study of the spectral problem for the operator

$$\mathcal{L}\,h := \frac{1}{\rho^\varepsilon(x)}\nabla\cdot\Big(A^\varepsilon(x)\nabla h(x)\Big). \tag{3.10}$$

The idea is to show that the study of the spectral problem for $\mathcal{L}$ is analogous to the study of the spectral problem for a Schrödinger-type operator. The essential calculations to follow are inspired by the calculations in [30, section 4.9, page 125]. Note that the operator $\mathcal{L}$ defined by (3.10) with zero Neumann boundary condition is a symmetric operator in $\mathrm{L}^2(\Omega;\rho^\varepsilon)$, i.e.,

$$\int_{\mathbb{R}^d}\mathcal{L}\,h_1(x)h_2(x)\rho^\varepsilon(x)\,\mathrm{d}x = \int_{\mathbb{R}^d}\mathcal{L}\,h_2(x)h_1(x)\rho^\varepsilon(x)\,\mathrm{d}x$$

for all $h_1, h_2 \in \mathrm{L}^2(\mathbb{R}^d;\rho^\varepsilon)$.

Let us now define the operator

$$\mathcal{H}\,h := \sqrt{\rho^\varepsilon(x)}\,\mathcal{L}\left(\frac{h}{\sqrt{\rho^\varepsilon(x)}}\right) = \frac{1}{\sqrt{\rho^\varepsilon(x)}}\nabla\cdot\left(\rho^\varepsilon(x)\Sigma^\varepsilon(x)\nabla\left(\frac{h}{\sqrt{\rho^\varepsilon(x)}}\right)\right) \tag{3.11}$$

with the coefficient

$$\Sigma^\varepsilon(x) := \frac{A^\varepsilon(x)}{\rho^\varepsilon(x)}.$$

An algebraic manipulation yields

$$\mathcal{H}\, h = \nabla \cdot \Big(\Sigma^\varepsilon(x)\nabla h\Big) + W^\varepsilon(x)\, h$$

with

$$W^\varepsilon(x) := \frac{1}{\sqrt{\rho^\varepsilon(x)}}\nabla \cdot \left(A^\varepsilon(x)\nabla\left(\frac{1}{\sqrt{\rho^\varepsilon(x)}}\right)\right).$$

In our setting, with the high contrast coefficients A^ε and ρ^ε from (2.10)–(2.9), the coefficients Σ^ε and W^ε become

$$\Sigma^\varepsilon(x) = \begin{cases} \mathrm{Id} & \text{for } x \in \Omega \setminus B_\varepsilon, \\ \varepsilon^2\, \frac{\beta}{\eta}\left(\frac{x}{\varepsilon}\right) & \text{for } x \in B_\varepsilon \end{cases}$$

and

$$W^\varepsilon(x) = \begin{cases} 0 & \text{for } x \in \Omega \setminus B_\varepsilon, \\ \varepsilon^2\, \nabla \cdot \left(\beta\left(\frac{x}{\varepsilon}\right) \nabla\left(\frac{1}{\sqrt{\eta}}\left(\frac{x}{\varepsilon}\right)\right)\right) & \text{for } x \in B_\varepsilon. \end{cases}$$

By definition (3.11), the operators $\mathcal{L}$ and $\mathcal{H}$ are unitarily equivalent. Hence they have the same eigenvalues. Note that the operator $\mathcal{H}$ is a Schrödinger-type operator where the coefficients are of high contrast.

By the Rayleigh–Ritz criterion, we have the characterization

$$\mu_k^\varepsilon \le \frac{\int_\Omega \Sigma^\varepsilon(x)\nabla\varphi(x)\cdot\nabla\varphi(x)\,\mathrm{d}x + \int_\Omega W^\varepsilon(x)\,|\varphi(x)|^2\,\mathrm{d}x}{\int_\Omega |\varphi(x)|^2\,\mathrm{d}x},$$

where $\varphi \not\equiv 0$ and is orthogonal to first $k-1$ Neumann eigenfunctions $\left\{\varphi_1^\varepsilon, \ldots, \varphi_{k-1}^\varepsilon\right\}$. Note that, in particular, for $k = 2$ (i.e., the first nonzero eigenvalue), we have

$$\|\varphi\|^2_{\mathrm{L}^2(\Omega)}\ \mu_2^\varepsilon \le \int_\Omega \Sigma^\varepsilon(x)\nabla\varphi(x)\cdot\nabla\varphi(x)\,\mathrm{d}x + \int_{B_\varepsilon} W^\varepsilon(x)\varphi(x)\,\mathrm{d}x \tag{3.12}$$

with $\varphi \in \mathrm{H}^1(\Omega)$ such that

$$\int_\Omega \varphi(x)\,\mathrm{d}x = 0.$$

Note that we have used the fact that $W^\varepsilon(x)$ is supported on B_ε. Note further that

$$W^\varepsilon(x) = \varepsilon^2\left\{\frac{1}{\varepsilon^2}\beta\left(\frac{x}{\varepsilon}\right) : \left[\nabla^2\left(\frac{1}{\sqrt{\eta}}\right)\right]\left(\frac{x}{\varepsilon}\right) + \frac{1}{\varepsilon^2}\left[\nabla\beta\right]\left(\frac{x}{\varepsilon}\right)\cdot\left[\nabla\left(\frac{1}{\sqrt{\eta}}\right)\right]\left(\frac{x}{\varepsilon}\right)\right\} = \mathcal{O}(1) \tag{3.13}$$

if we assume $\beta \in \mathrm{W}^{1,\infty}(B_1;\mathbb{R}^{d\times d})$ and $\eta \in \mathrm{W}^{2,\infty}(B_1)$.

Note further that the spectral problem (3.3) comes with the following characterization of the first nonzero eigenvalue (again by the Rayleigh–Ritz criterion):

$$\|\varphi\|^2_{\mathrm{L}^2(\Omega)}\ \mu_2 \le \int_\Omega \nabla\varphi(x)\cdot\nabla\varphi(x)\,\mathrm{d}x \tag{3.14}$$

with $\varphi \in \mathrm{H}^1(\Omega)$ such that

$$\int_\Omega \varphi(x)\,\mathrm{d}x = 0.$$

Subtracting (3.12) from (3.14) yields

$$\|\varphi\|^2_{\mathrm{L}^2(\Omega)}\ (\mu_2 - \mu_2^\varepsilon) \le \int_{B_\varepsilon} \left(\mathrm{Id} - \varepsilon^2 \frac{1}{\eta}\left(\frac{x}{\varepsilon}\right)\beta\left(\frac{x}{\varepsilon}\right)\right)\nabla\varphi(x)\cdot\nabla\varphi(x)\,\mathrm{d}x + \int_{B_\varepsilon} W^\varepsilon(x)\varphi(x)\,\mathrm{d}x.$$

Let us now take the test function φ to be the normalized eigenfunction $\varphi_2(x)$ associated with the first nonzero eigenvalue μ_2 for the Neumann Laplacian:

$$|\mu_2 - \mu_2^\varepsilon| \le \left|\int_{B_\varepsilon} \left(\mathrm{Id} - \varepsilon^2 \frac{1}{\eta}\left(\frac{x}{\varepsilon}\right)\beta\left(\frac{x}{\varepsilon}\right)\right)\nabla\varphi_2(x)\cdot\nabla\varphi_2(x)\,\mathrm{d}x + \int_{B_\varepsilon} W^\varepsilon(x)\varphi_2(x)\,\mathrm{d}x\right|.$$

Using the observation (3.13) that the potential W^ε is of $\mathcal{O}(1)$ and that the Neumann eigenfunctions are bounded in $\mathrm{W}^{p,\infty}$ for any $p < \infty$ [17], we have proved that

$$|\mu_2 - \mu_2^\varepsilon| \lesssim \varepsilon^d.$$

In this subsection, we have essentially proved the following result.

PROPOSITION 9. *Suppose that the high contrast conductivity-density pair $A^\varepsilon, \rho^\varepsilon$ is given by* (2.10)–(2.9) *with $\beta \in \mathrm{W}^{1,\infty}(B_1;\mathbb{R}^{d\times d})$ and $\eta \in \mathrm{W}^{2,\infty}(B_1)$. Let μ_2^ε and μ_2 be the first nonzero eigenvalues associated with the Neumann spectral problems* (3.6) *and* (3.3)*, respectively. Then we have*

$$|\mu_2 - \mu_2^\varepsilon| \lesssim \varepsilon^d. \tag{3.15}$$

Hence, as a corollary to the above result, we can deduce that the decay rate for the homogeneous transient problem (3.1) and that for the high contrast transient problem (3.4) are close to each other in the $\varepsilon \ll 1$ regime.

4. Near-cloaking result. In this section, we will prove the main result of this paper, i.e., Theorem 2. To that end, we first consider the steady-state problem associated with the homogeneous heat equation (2.5). More precisely, for the unknown $u^{\mathrm{eq}}_{\mathrm{hom}}(x)$, consider

$$\begin{aligned} -\Delta u^{\mathrm{eq}}_{\mathrm{hom}}(x) &= f(x) \qquad \text{in } \Omega,\\ \nabla u^{\mathrm{eq}}_{\mathrm{hom}}\cdot\mathbf{n}(x) &= g(x) \qquad \text{on } \partial\Omega,\\ \int_\Omega u^{\mathrm{eq}}_{\mathrm{hom}}(x)\,\mathrm{d}x &= 0. \end{aligned} \tag{4.1}$$

Note that the last line of (4.1) is to ensure that we solve for $u^{\mathrm{eq}}_{\mathrm{hom}}(x)$ uniquely. Here we assume that the source terms are admissible in the sense of (2.12). This guarantees the solvability of the above elliptic boundary value problem.

Next, we record a corollary to Proposition 6 which says how quickly the solution $u_{\mathrm{hom}}(t,x)$ to the homogeneous problem (2.5) tends to its equilibrium state.

COROLLARY 10. *Let $u_{\mathrm{hom}}(t,x)$ be the solution to* (2.5)*, and let $u^{\mathrm{eq}}_{\mathrm{hom}}(x)$ be the solution to the steady-state problem* (4.1)*. Suppose the source terms $f(x)$, $g(x)$ and the initial datum $u^{\mathrm{in}}(x)$ are admissible in the sense of* (2.12)–(2.13)*. Then*

$$\|u_{\mathrm{hom}}(t,\cdot) - u^{\mathrm{eq}}_{\mathrm{hom}}(\cdot)\|_{\mathrm{H}^1(\Omega)} \le e^{-\gamma t}\left\|u^{\mathrm{in}} - u^{\mathrm{eq}}_{\mathrm{hom}}\right\|_{\mathrm{H}^1(\Omega)} \tag{4.2}$$

for some positive constant γ.

Proof. Define a function $w(t,x) := u_{\text{hom}}(t,x) - u^{\text{eq}}_{\text{hom}}(x)$. We have that the function $w(t,x)$ satisfies the evolution equation

$$\begin{aligned} \partial_t w &= \Delta w && \text{in } (0,\infty)\times\Omega,\\ \nabla w\cdot \mathbf{n}(x) &= 0 && \text{on } (0,\infty)\times\partial\Omega,\\ w(0,x) &= u^{\text{in}}(x) - u^{\text{eq}}_{\text{hom}}(x) && \text{in } \Omega, \end{aligned}$$

which is the same as (3.1). The estimate (4.2) is simply deduced from Proposition 6 (see, in particular, (3.2)). ∎

Now we record a result, as a corollary to Proposition 7, demonstrating how quickly the solution $u^\varepsilon(t,x)$ to the defect problem with high contrast coefficients (2.11) tends to its equilibrium state. Consider the steady-state problem associated with the defect problem (2.11). More precisely, for the unknown $u^\varepsilon_{\text{eq}}(x)$, consider the elliptic boundary value problem

$$\begin{aligned} -\nabla\cdot\left(A^\varepsilon(x)\nabla u^\varepsilon_{\text{eq}}\right) &= f(x) && \text{in } \Omega,\\ \nabla u^\varepsilon_{\text{eq}}\cdot\mathbf{n}(x) &= g(x) && \text{on } \partial\Omega,\\ \int_\Omega \rho^\varepsilon(x) u^\varepsilon_{\text{eq}}(x)\,\mathrm{d}x &= 0. \end{aligned} \tag{4.3}$$

Note that the normalization condition in (4.3) makes use of the density coefficient $\rho^\varepsilon(x)$ defined by (2.9).

COROLLARY 11. *Let $u^\varepsilon(t,x)$ be the solution to* (2.11)*, and let $u^\varepsilon_{\text{eq}}(x)$ be the solution to the steady-state problem* (4.3)*. Suppose the source terms $f(x)$, $g(x)$ and the initial datum $u^{\text{in}}(x)$ are admissible in the sense of* (2.12)–(2.13)*. Suppose further that* $\operatorname{supp} u^{\text{in}} \subset \Omega\setminus B_2$*. Then*

(4.4)
$$\begin{aligned} &\left\|u^\varepsilon(t,\cdot) - u^\varepsilon_{\text{eq}}(\cdot)\right\|_{\mathrm{H}^1(\Omega)}\\ &\qquad\le e^{-\gamma_\varepsilon t}\left(\frac{1}{\varepsilon^d}\left\|u^{\text{in}} - u^\varepsilon_{\text{eq}}\right\|_{\mathrm{L}^2(\Omega)} + \frac{1}{\varepsilon^{\frac{d-2}{2}}}\left\|\nabla\left(u^{\text{in}} - u^\varepsilon_{\text{eq}}\right)\right\|_{\mathrm{L}^2(\Omega)}\right). \end{aligned}$$

Proof. Define a function $w^\varepsilon(t,x) := u^\varepsilon(t,x) - u^\varepsilon_{\text{eq}}(x)$. We have that the function $w^\varepsilon(t,x)$ satisfies the evolution equation

$$\begin{aligned} \rho^\varepsilon(x)\partial_t w^\varepsilon &= \nabla\cdot\left(A^\varepsilon(x)\nabla w^\varepsilon\right) && \text{in } (0,\infty)\times\Omega,\\ \nabla w^\varepsilon\cdot\mathbf{n}(x) &= 0 && \text{on } (0,\infty)\times\partial\Omega,\\ w^\varepsilon(0,x) &= u^{\text{in}}(x) - u^\varepsilon_{\text{eq}}(x) && \text{in } \Omega, \end{aligned}$$

which is the same as (3.4). By assumption, the initial datum u^{in} is supported away from B_2. This along with the admissibility assumption (2.13) implies that the weighted average $\mathfrak{m}^\varepsilon$ defined in Proposition 7 vanishes. Then the estimate (4.4) is simply deduced from Proposition 7 (see, in particular, (3.5)). ∎

Proof of Theorem 2. From the triangle inequality, we have

$$\|u^\varepsilon(t,\cdot)-u_{\mathrm{hom}}(t,\cdot)\|_{\mathrm{H}^{\frac{1}{2}}(\partial\Omega)} \le \left\|u^\varepsilon(t,\cdot)-u^\varepsilon_{\mathrm{eq}}(\cdot)\right\|_{\mathrm{H}^{\frac{1}{2}}(\partial\Omega)} + \left\|u^\varepsilon_{\mathrm{eq}}-u^{\mathrm{eq}}_{\mathrm{hom}}\right\|_{\mathrm{H}^{\frac{1}{2}}(\partial\Omega)} + \|u^{\mathrm{eq}}_{\mathrm{hom}}(\cdot)-u_{\mathrm{hom}}(t,\cdot)\|_{\mathrm{H}^{\frac{1}{2}}(\partial\Omega)}.$$

The boundary trace inequality gives the existence of a constant $\mathfrak{c}_\Omega$—depending only on the domain Ω—such that

$$\|u^\varepsilon(t,\cdot)-u_{\mathrm{hom}}(t,\cdot)\|_{\mathrm{H}^{\frac{1}{2}}(\partial\Omega)} \le \mathfrak{c}_\Omega\left\|u^\varepsilon(t,\cdot)-u^\varepsilon_{\mathrm{eq}}(\cdot)\right\|_{\mathrm{H}^1(\Omega)} + \left\|u^\varepsilon_{\mathrm{eq}}-u^{\mathrm{eq}}_{\mathrm{hom}}\right\|_{\mathrm{H}^{\frac{1}{2}}(\partial\Omega)} + \mathfrak{c}_\Omega\|u^{\mathrm{eq}}_{\mathrm{hom}}(\cdot)-u_{\mathrm{hom}}(t,\cdot)\|_{\mathrm{H}^1(\Omega)}.$$

Using the result of Corollaries 10 and 11 and the DtN estimate from [11, Lemma 2.2, page 305] (see also [22, Proposition 1]), we get that the right-hand side of the above inequality is bounded from above by

$$\mathfrak{c}_\Omega e^{-\gamma_\varepsilon t}\left(\frac{1}{\varepsilon^d}\left\|u^{\mathrm{in}}-u^\varepsilon_{\mathrm{eq}}\right\|_{\mathrm{L}^2(\Omega)} + \frac{1}{\varepsilon^{\frac{d-2}{2}}}\left\|\nabla\left(u^{\mathrm{in}}-u^\varepsilon_{\mathrm{eq}}\right)\right\|_{\mathrm{L}^2(\Omega)}\right) + \varepsilon^d\left(\|f\|_{\mathrm{L}^2(\Omega)}+\|g\|_{\mathrm{L}^2(\partial\Omega)}\right) + \mathfrak{c}_\Omega e^{-\gamma t}\left\|u^{\mathrm{in}}-u^{\mathrm{eq}}_{\mathrm{hom}}\right\|_{\mathrm{H}^1(\Omega)}.$$

Hence the existence of a time instant T follows such that for all $t \ge T$, we indeed have the estimate (2.14). ∎

Remark 12. We make some observations on why the admissibility assumption (2.13) and the assumption on the support of the initial datum in Corollary 11 were essential to our proof. In the absence of these assumptions, in the proof of Theorem 2, we will have to show that

$$\lim_{\varepsilon\to 0}\left|\mathfrak{m}^\varepsilon - \langle u^{\mathrm{in}}\rangle\right| = 0. \tag{4.5}$$

Let us compute the difference:

$$\mathfrak{m}^\varepsilon - \langle u^{\mathrm{in}}\rangle = \left(|\Omega\setminus B_\varepsilon| + \frac{\pi^{\frac{d}{2}}}{\Gamma\left(\frac{d}{2}+1\right)}\right)^{-1}\left\{\int_{\Omega\setminus B_\varepsilon} u^{\mathrm{in}}(x)\,\mathrm{d}x + \frac{1}{\varepsilon^d}\int_{B_\varepsilon} u^{\mathrm{in}}(x)\,\mathrm{d}x\right\} - \frac{1}{|\Omega|}\int_\Omega u^{\mathrm{in}}(x)\,\mathrm{d}x.$$

We have not managed to characterize all initial data that guarantee the asymptote (4.5). The difficulty of this task becomes apparent if you take initial data to be supported away from B_1 but not satisfying the zero mean assumption (2.13). Note that our assumption on the initial data in Corollary 11 guarantees the above difference is always zero, irrespective of the value of the parameter ε.

Remark 13. Our choice of the domain Ω containing B_2 is arbitrary, and Corollary 3 asserts that for any such arbitrary choice, the distance between the solutions u_{hom} and u_{cl} (measured in the $\mathrm{H}^{\frac{1}{2}}(\partial\Omega)$-norm) can be made as small as we wish, provided we engineer appropriate cloaking coefficients (for instance via a homogenization approach)—see (2.7) and (2.8)—in the annulus $B_2\setminus B_1$. This is the notion of *near-cloak*. Unlike the *perfect cloaking* strategies which demand equality between u_{hom}

and $u_{\rm cl}$ everywhere outside B_2, near-cloak strategies only ask for them to be close in certain norm topologies. Near-cloaking strategies are what matter in practice.

We can still pose the thermal cloaking question in full space $\mathbb{R}^d$. In this scenario, the norm of choice becomes the one in $\mathrm{H}^1_{\rm loc}(\mathbb{R}^d \setminus B_2)$. More precisely, for any compact set $K \subset \mathbb{R}^d \setminus B_2$, we can prove

$$\|u^\varepsilon(t,\cdot) - u_{\rm hom}(t,\cdot)\|_{\mathrm{H}^1(K)} \lesssim \varepsilon^{\frac{d}{2}} \qquad \text{for } t \gg 1.$$

4.1. Layered cloaks. Advancing an idea from [12], we develop a transformation media theory for thermal layered cloaks, which are of practical importance in thin-film solar cells for energy harvesting in the photovoltaic industry. The basic principle behind this construction is the following observation.

PROPOSITION 14. *Let the spatial domain $\Omega := (-3,3)^2$. Let the density conductivity pair $\rho \in \mathrm{L}^\infty(\Omega;\mathbb{R})$, $A \in \mathrm{L}^\infty(\Omega;\mathbb{R}^{2\times 2})$ be such that they are $(-3,3)$-periodic in the x_1 variable. Consider a smooth invertible map $\mathtt{f}(x_2) : \mathbb{R} \mapsto \mathbb{R}$ such that $\mathtt{f}(x_2) = x_2$ for $|x_2| > 2$. Assume further that $\mathtt{f}'(x_2) \geq C > 0$ for a.e. $x_2 \in (-3,3)$. Take the mapping $\mathbb{F} : \Omega \mapsto \Omega$ defined by $\mathbb{F}(x_1,x_2) = (x_1, \mathtt{f}(x_2))$. Then $u(t,x_1,x_2)$ is a $(-3,3)$-periodic solution (in the x_1 variable) to*

$$\rho(x)\partial_t u = \nabla_x \cdot \Big(A(x)\nabla_x u\Big) + h(x) \qquad \text{for } (t,x) \in (0,\infty)\times\Omega$$

if and only if $v = u \circ \mathbb{F}^{-1}$ is a $(-3,3)$-periodic solution (in the $y_1 = x_1$ variable) to

$$\mathbb{F}^*\rho(y)\,\partial_t v = \nabla \cdot \Big(\mathbb{F}^* A(y)\nabla v\Big) + \mathbb{F}^* f(y) \qquad \text{for } (t,y) \in (0,\infty)\times\Omega,$$

where the coefficients are given by

$$\begin{aligned}
\mathbb{F}^*\rho(y_1,y_2) &= \frac{1}{\mathtt{f}'(x_2)}\rho(x_1,x_2);\\
\mathbb{F}^* h(t,y_1,y_2) &= \frac{1}{\mathtt{f}'(x_2)} h(t,x_1,x_2);\\
\mathbb{F}^* A(y_1,y_2) &= \begin{pmatrix} \frac{1}{\mathtt{f}'(x_2)}A_{11}(x_1,x_2) & A_{12}(x_1,x_2) \\ \frac{1}{\mathtt{f}'(x_2)}A_{21}(x_1,x_2) & \mathtt{f}'(x_2)A_{22}(x_1,x_2)\end{pmatrix}
\end{aligned} \tag{4.6}$$

with the understanding that the right-hand sides in (4.6) *are computed at $(x_1,x_2) = (y_1, \mathtt{f}^{-1}(y_2))$. Furthermore, we have*

$$u(t,x_1,x_2) = v(t,x_1,x_2) \qquad \text{for } |x_2| \geq 2.$$

Next, we prove a near-cloaking result in this present setting of layered cloaks. It concerns the following evolution problems: the homogeneous problem

$$\begin{aligned}
\partial_t u_{\rm hom}(t,x) &= \Delta u_{\rm hom}(t,x) + f(x) && \text{in } (0,\infty)\times\Omega,\\
\nabla u_{\rm hom}(x_1,\pm 3)\cdot \mathbf{n}(x_1,\pm 3) &= g(x_1) && \text{on } (0,\infty)\times(-3,3),\\
u_{\rm hom}(-3,x_2) &= u_{\rm hom}(3,x_2) && \text{for } x_2 \in (-3,3),\\
u_{\rm hom}(0,x) &= u^{\rm in}(x) && \text{in } \Omega
\end{aligned} \tag{4.7}$$

and the layered cloak problem

$$
\begin{aligned}
\rho_{\mathrm{cl}}(x)\partial_t u_{\mathrm{cl}} &= \nabla\cdot\Big(A_{\mathrm{cl}}(x)\nabla u_{\mathrm{cl}}\Big)+f(x) && \text{in } (0,\infty)\times\Omega,\\
\nabla u_{\mathrm{cl}}(x_1,\pm 3)\cdot\mathbf{n}(x_1,\pm 3) &= g(x_1) && \text{on } (0,\infty)\times(-3,3),\\
u_{\mathrm{cl}}(-3,x_2) &= u_{\mathrm{cl}}(3,x_2) && \text{for } x_2\in(-3,3),\\
u_{\mathrm{cl}}(0,x) &= u^{\mathrm{in}}(x) && \text{in } \Omega,
\end{aligned}
\tag{4.8}
$$

where the coefficients ρ_{cl} and A_{cl} in (4.8) are defined using the Lipschitz mapping $(x_1,x_2)\mapsto(x_1,\mathtt{f}_\varepsilon(x_2))$ with

$$
\mathtt{f}_\varepsilon(x_2):=\begin{cases} x_2 & \text{for } |x_2|>2,\\ \left(\frac{2-2\varepsilon}{2-\varepsilon}+\frac{|x_2|}{2-\varepsilon}\right)\frac{x_2}{|x_2|} & \text{for } 1\le|x_2|\le 2,\\ \frac{x_2}{\varepsilon} & \text{for } |x_2|<1.\end{cases}
\tag{4.9}
$$

The precise construction of the layered cloaks is as follows:

$$
\rho_{\mathrm{cl}}(x_1,x_2)=\begin{cases} 1 & \text{for } |x_2|>2,\\ \mathcal{F}_\varepsilon^* 1 & \text{for } 1<|x_2|<2,\\ \eta(x_1,x_2) & \text{for } |x_2|<1\end{cases}
\tag{4.10}
$$

and

$$
A_{\mathrm{cl}}(x_1,x_2)=\begin{cases} \mathrm{Id} & \text{for } |x_2|>2,\\ \mathcal{F}_\varepsilon^*\mathrm{Id} & \text{for } 1<|x_2|<2,\\ \beta(x_1,x_2) & \text{for } |x_2|<1,\end{cases}
\tag{4.11}
$$

where the push-forward maps are defined in (4.6). The density coefficient $\eta(x)$ in (4.10) is any arbitrary real positive function. The conductivity coefficient $\beta(x)$ in (4.11) is any arbitrary bounded positive definite matrix.

Let us make the observation that the cloaking coefficients ρ_{cl} and A_{cl} given by (4.10) and (4.11), respectively, can be treated as push-forward outcomes (via the push-forward maps (4.6)) of the following defect coefficients:

$$
\rho^\varepsilon(x)=\begin{cases} 1 & \text{for } \varepsilon<|x_2|<2,\\ \frac{1}{\varepsilon}\eta\left(x_1,\frac{x_2}{\varepsilon}\right) & \text{for } |x_2|<\varepsilon\end{cases}
\tag{4.12}
$$

and

$$
A^\varepsilon(x)=\begin{cases} \mathrm{Id} & \text{for } \varepsilon<|x_2|<2,\\ \begin{pmatrix} \frac{1}{\varepsilon}\beta_{11}\left(x_1,\frac{x_2}{\varepsilon}\right) & \beta_{12}\left(x_1,\frac{x_2}{\varepsilon}\right)\\ \beta_{21}\left(x_1,\frac{x_2}{\varepsilon}\right) & \varepsilon\beta_{22}\left(x_1,\frac{x_2}{\varepsilon}\right)\end{pmatrix} & \text{for } |x_2|<\varepsilon.\end{cases}
\tag{4.13}
$$

It then follows from Proposition 14 that comparing u_{hom} and u_{cl} is equivalent to comparing u_{hom} and u^ε, where $u^\varepsilon(t,x)$ solves the following defect problem with the

aforementioned ρ^ε and A^ε as coefficients:

$$
\begin{aligned}
\rho^\varepsilon(x)\partial_t u^\varepsilon &= \nabla\cdot\left(A^\varepsilon(x)\nabla u^\varepsilon\right)+f(x) && \text{in } (0,\infty)\times\Omega,\\
\nabla u^\varepsilon(x_1,\pm 3)\cdot\mathbf{n}(x_1,\pm 3) &= g(x_1) && \text{on } (0,\infty)\times(-3,3),\\
u^\varepsilon(-3,x_2) &= u_{\mathrm{cl}}(3,x_2) && \text{for } x_2\in(-3,3),\\
u^\varepsilon(0,x) &= u^{\mathrm{in}}(x) && \text{in } \Omega.
\end{aligned}
\tag{4.14}
$$

THEOREM 15. *Let $u^\varepsilon(t,x)$ be the solution to the defect problem* (4.14) *with high contrast coefficients* (4.12)–(4.13)*, and let $u_{\mathrm{hom}}(t,x)$ be the solution to the homogeneous conductivity problem* (4.7)*. Then there exists a time instant $T<\infty$ such that for all $t\geq T$, we have*

$$
\|u^\varepsilon(t,\cdot)-u_{\mathrm{hom}}(t,\cdot)\|_{\mathrm{H}^{\frac{1}{2}}(\Gamma)}\lesssim\varepsilon^2. \tag{4.15}
$$

The proof is similar to the proof of Theorem 2. More specifically, we show first that the solutions to the transient problems (4.14) and (4.7) converge exponentially fast to their corresponding equilibrium states. We can then adapt the energy approach in the proof of [11] to show that the equilibrium states are ε^2 close in the $\mathrm{H}^{\frac{1}{2}}(\Gamma)$-norm. We note that our analysis of near-cloaking for thermal layered cloaks can be easily adapted to electrostatic and electromagnetic cases. It might also find interesting applications in Earth science for seismic tomography, in which case one could utilize results in [4] to prove near-cloaking results related to imaging the subsurface of the Earth with seismic waves produced by earthquakes.

5. Numerical results. This section deals with the numerical tests done in support of the theoretical results in the paper. The tests designed in the subsections to follow make some observations with regards to the near-cloaking scheme designed in the previous sections of this paper. The numerical simulations are done in one, two, and three spatial dimensions. It seems natural to start with the one-dimensional case, but as it turns out (see subsection 4.1), the physical problem of interest for a one-dimensional (so-called layered) cloak requires a two-dimensional computational domain, and thus we start with the two-dimensional case. We refer the reader to [12] for the precise physical setup and importance of the layered cloak described in the context of Maxwell's equations (this is easily translated into the language of conductivity equations). These numerical simulations were performed with the finite element software COMSOL MULTIPHYSICS.

We choose the spatial domain to be a square $\Omega:=(-3,3)^2$. We take the bulk source $f(x)$, the Neumann datum $g(x)$, and the initial datum $u^{\mathrm{in}}(x)$ to be smooth and such that $\operatorname{supp} f\subset\Omega\setminus B_2$, $\operatorname{supp} u^{\mathrm{in}}\subset\Omega\setminus B_2$. We further assume that

$$
\int_\Omega f(x)\,\mathrm{d}x=0,\qquad \int_{\partial\Omega} g(x)\,\mathrm{d}\sigma(x)=0,\qquad \int_\Omega u^{\mathrm{in}}(x)\,\mathrm{d}x=0.
$$

This guarantees that the data is admissible in the sense of (2.12)–(2.13).

5.1. Near-cloaking. The numerical experiments in this subsection analyze the sharpness of the near-cloaking result (Theorem 2) in this paper. We solve the initial-boundary value problem for the unknown $u^\varepsilon(t,x)$:

$$
\rho^\varepsilon(x)\frac{\partial u^\varepsilon}{\partial t}=\nabla\cdot\left(A^\varepsilon(x)\nabla u^\varepsilon\right)+f(x)\qquad\text{in } (0,\infty)\times\Omega \tag{5.1}
$$

with the density-conductivity coefficients

$$\rho^\varepsilon(x),\, A^\varepsilon(x) = \begin{cases} 1, & \mathrm{Id} & \text{for } x \in \Omega \setminus B_\varepsilon, \\ \frac{1}{\varepsilon^2}\eta\left(\frac{x}{\varepsilon}\right), & \beta\left(\frac{x}{\varepsilon}\right) & \text{for } x \in B_\varepsilon. \end{cases}$$

Note that in two dimensions, there is no high contrast in the conductivity coefficient $A^\varepsilon(x)$. There is, however, contrast in the density coefficient $\rho^\varepsilon(x)$. The evolution (5.1) is supplemented by the Neumann datum

$$g(x_1, x_2) = \begin{cases} -3 & \text{for } x_1 = \pm 3, \\ 0 & \text{for } x_2 = \pm 3 \end{cases}$$

and the initial datum

$$u^{\mathrm{in}}(x_1, x_2) = \begin{cases} x_1 x_2 & \text{for } x \in \Omega \setminus B_2, \\ 0 & \text{for } x \in B_\varepsilon. \end{cases}$$

The bulk force in (5.1) is taken to be

$$f(x_1, x_2) = \begin{cases} \sqrt{x_1^2 + x_2^2}\,\sin(x_1)\sin(x_2) - 2 & \text{for } x \in \Omega \setminus B_2, \\ 0 & \text{for } x \in B_\varepsilon. \end{cases}$$

We next solve the initial-boundary value problem (Neumann) for $u_{\mathrm{hom}}(t, x)$ with the above data:

$$\partial_t u_{\mathrm{hom}}(t, x) = \Delta u_{\mathrm{hom}}(t, x) + f(x) \qquad \text{in } (0, \infty) \times \Omega.$$

Let us define

$$\mathcal{G}_\varepsilon(t) := \frac{\|u^\varepsilon(t, \cdot) - u_{\mathrm{hom}}(t, \cdot)\|_{\mathrm{L}^2(\partial\Omega)}}{\varepsilon^d \left(\|u^{\mathrm{in}}\|_{\mathrm{H}^1} + \|f\|_{\mathrm{L}^2(\Omega)} + \|g\|_{\mathrm{L}^2(\partial\Omega)} \right)}. \tag{5.2}$$

We compute the function $\mathcal{G}_\varepsilon(t)$ defined by (5.2) as a function of time for various values of ε (see Figure 1) and numerically observe that after $110s$, $\mathcal{G}_\varepsilon(t)$ reaches an asymptote that tends towards a numerical value close to 8.6 when ε gets smaller, in agreement with theoretical predictions of Theorem 2 for space dimension $d = 2$. The simulations were performed using an adaptive mesh of the domain Ω consisting of 2×10^5 nodal elements (with at least 10^2 elements in the small defect when $\varepsilon = 10^{-4}$) and a numerical solver based on the backward differential formula (BDF) solver with initial time step $10^{-5}s$, maximum time step $10^{-1}s$, and minimum and maximum BDF orders of 1 and 5, respectively. Many test cases were run for various values of β (including anisotropic conductivity) and η in the small inclusion, and we report some representative curves in Figure 1.

5.2. Contour plots. Let us start with the contour plots for the layered cloak developed in subsection 4.1; see Figure 2. More precisely, we compare solutions u_{hom} and u_{cl} to the evolution problems (4.7) and (4.8), respectively, where periodic boundary conditions are imposed at the boundary $x_1 = \pm 3$ and homogeneous Neumann data at the boundary $x_2 = \pm 3$. Here we illustrate the layered cloak by numerically

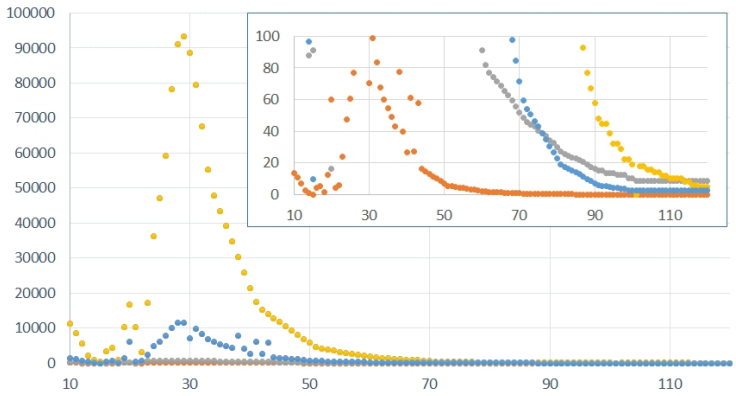

FIG. 1. *Numerical results for $\mathcal{G}_\varepsilon(t)$ vs. time t (with a source outside B_2): Same parameters as in Figure 3 for a small defect of radius $\varepsilon = 10^{-1}$ (orange), $\varepsilon = 10^{-2}$ (grey), $\varepsilon = 10^{-3}$ (blue), and $\varepsilon = 10^{-4}$ (yellow) and diffusivity $\beta(x/\varepsilon) = 2$ Id and density $\varepsilon^{-2}\eta(x/\varepsilon) = 2\varepsilon^{-2}$ in the inclusion B_ε. Horizontal linear scale of time $t \in [0, 110]$ s. Vertical scale of $\varepsilon^{-2}|\|u^\varepsilon(t,.)\|_{L^2(\partial\Omega)} - \|u_{hom}(t,.)\|_{L^2(\partial\Omega)}|$ is a representation of $\mathcal{G}_\varepsilon(t)$. Insert shows a zoom-in. Color is available online only.*

solving an equation for the unknown $u(t, x_1, x_2)$, but the conductivity and density only depend upon the x_2 variable. We take the source to be

$$f(x_1, x_2) = \begin{cases} x_2 \sin(x_2) & \text{for } x_2 \in (-3, -2) \cup (2, 3), \\ 0 & \text{for } x_2 \in (-2, 2), \end{cases}$$

and the initial datum is taken to be

$$u^{\text{in}}(x_1, x_2) = \begin{cases} x_2 & \text{for } x_2 \in (-3, -2) \cup (2, 3), \\ 0 & \text{for } x_2 \in (-2, 2). \end{cases}$$

Following the layered cloak construction in (4.11), we take the cloaking conductivity to be the push-forward of identity in the cloaking strip:

$$A_{\text{cl}}(x_1, x_2) = \text{diag}\left(2 - \varepsilon, \frac{1}{2 - \varepsilon}\right) \qquad \text{for } 1 < |x_2| < 2.$$

We report in Figure 2 some numerical results that exemplify the high level of control of the heat flux with a layered cloak: in the upper panels (a), (b), (c), one can see snapshots at representative time steps ($t = 0$, 1, and 4s) of a typical one-dimensional diffusion process in a homogeneous medium for a given source with a support outside $x_2 \in (-2, 2)$. When we compare the temperature field at the initial time step in (a) with that when we replace the homogeneous medium by a layered cloak in $1 < |x_2| < 2$ in (d), we note no difference. However, some noticeable differences are noted for the temperature field between the homogeneous medium and the cloak when comparing (b) with (e) and (c) with (f). The gradient of the temperature field is dramatically decreased in the invisibility region $x_2 \in (-1, 1)$, leading to an almost uniform (but nonzero) temperature field therein, and this is compensated by an enhanced gradient of temperature within the cloak in $1 < |x_2| < 2$. One notes that the increased flux in $1 < |x_2| < 2$ might be useful to improve efficiency of solar cells in photovoltaics.

Our next experiment is to compare the homogeneous solution and the cloaked solution where the cloaking coefficients are constructed using the push-forward maps

as in (2.7)–(2.8). The data $(f,\ g,\ u^{\text{in}})$ are chosen as in subsection 5.1. We report in Figure 3 some numerical computations performed in COMSOL MULTIPHYSICS that illustrate the strong similarity between the temperature fields in homogeneous (a)–(d), small defect (e)–(h), and cloaked (i)–(l) problems. Obviously, the fields are identical outside B_2 at the initial time step; then they differ most outside B_2 at small time step $t = 1s$ (see (b), (f), (j)) and become more and more similar with increasing time steps; see (c), (g), (k) and (d), (h), (l). These qualitative observations are consistent with the near-cloaking result, Theorem 2, of this paper.

We have also performed a similar experiment in three dimensions; see Figure 4. We refer the reader to the caption in Figure 4 for the parameters considered in the three-dimensional problem. Note that for these three-dimensional computations, we mesh the cubical domain with $40,000$ nodal elements, we take time steps of $0.1s$, and we use the BDF solver with initial time step $0.01s$, maximum time step $0.1s$, and minimum and maximum BDF orders of 1 and 3, respectively. We use a desktop with 32 GB of RAM memory, and a computation run takes around 1 hour for a time interval between 0.1 and $10s$. We can neither study long time behaviors, nor solve the high contrast small defect problem in three dimensions, as this would require more computational resources. Nevertheless, our three-dimensional computations suggest that there is a strong similarity between the temperature fields in homogeneous and cloaked problems outside B_2. Note also that we consider a source not vanishing inside B_2, which motivates further theoretical analysis for sources with a support in the overall domain Ω.

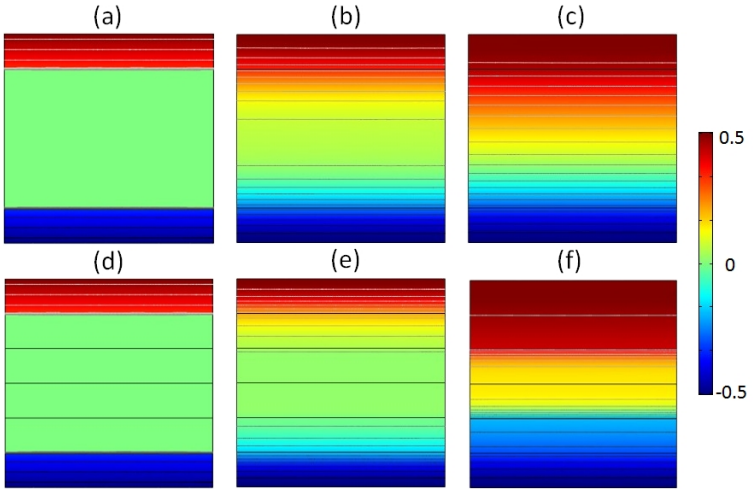

FIG. 2. *Contour plots of a layered cloak (with a source outside $x_2 \in (-2,2)$): $f(x) = x_2 \sin(x_2)$ for $x \in \{(x_1,x_2) : x_2 \in (-3,-2) \cup (2,3)\}$ and $f(x) = 0$ for $x_2 \in (-2,2)$. Upper panel: Plots of u for data $u^{in}(x) = x_2$ and $g(x) = 0$ for $x_2 = \pm 3$ and such that $u(-3,x_2) = u(3,x_2)$ (periodicity condition) for a homogeneous medium with diffusivity $A = 1$ at time steps $t = 0s$* (a), *$1s$* (b), *and $4s$* (c). *Lower panel: Same for the medium with diffusivity $A = 1$ outside $x_2 \in (-2,2)$ and a layered cloak inside $x_2 \in (-2,2)$ with diffusivity $A(x_2) = \text{diag}\big(\mathbb{A}_{11}(x_2), \frac{1}{\mathbb{A}_{11}(x_2)}\big)$ and density $\rho(x_2) = \mathbb{A}_{11}(x_2)$ with $\mathbb{A}_{11} = \varepsilon$ in $x_2 \in (-1,1)$ and $\mathbb{A}_{11} = 2 - \varepsilon$ in $1 < |x_2| < 2$ at time steps $t = 0s$* (d), *$1s$* (e), *and $4s$* (f).

5.3. Cloaking coefficients. The cloaking coefficients ρ_{cl} and A_{cl} in the annulus $B_2 \setminus B_1$ play all the essential roles in thermal cloaking phenomena. So, it is important

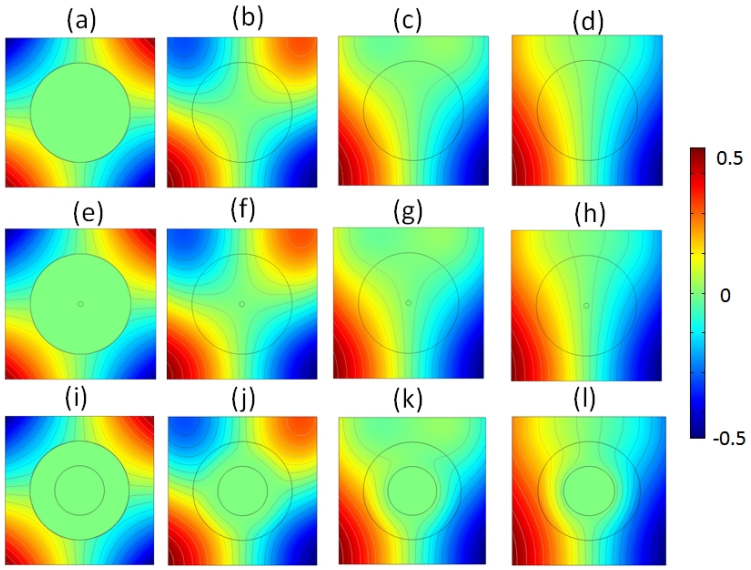

FIG. 3. *Contour plots of a two-dimensional cloak (with a source outside B_2): $f(x) = \sqrt{x_1^2 + x_2^2}\sin(x_1)\sin(x_2) - 2$ for $x \in \Omega \setminus B_2$ and $f(x) = 0$ for $x \in B_2$. Upper panel: Plots of u for data $u^{in}(x_1, x_2) = x_1 x_2$ and $g(x_1, x_2) = -3$ for $x_1 = \pm 3$ and 0 for $x_2 = \pm 3$ and diffusivity $A = 1$ at time steps $t = 0s$, $1s$, $4s$, $10s$, and $20s$. Middle panel: Same for a small defect of radius $\varepsilon = 10^{-1}$, density $\rho^\varepsilon = 2\varepsilon^{-2}$, and diffusivity $A^\varepsilon = 2$ Id. Lower panel: Same for a cloak.*

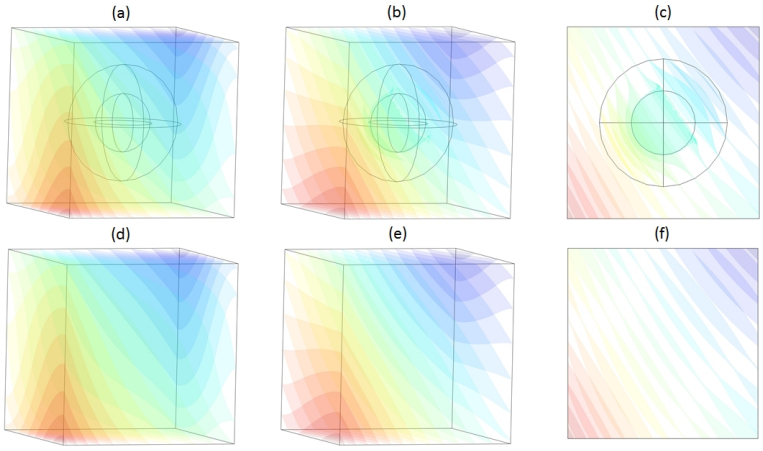

FIG. 4. *Numerical results for isosurface plots (source outside and inside B_2): $f_{cl}(x) = \sqrt{x_1^2 + x_2^2 + x_3^2}\sin(x_1)\sin(x_2)\sin(x_3)$ for $x \in \Omega$. Upper panel: Plots of u for data $u^{in}(x) = x_3$ and $g(x) = -3$ for $x_1 = \pm 3$ and $x_2 = \pm 3$ and 0 for $x_3 = \pm 3$ and diffusivity $A = 1$ outside a cloak defined as in (2.8) at time steps $t = 0.7s$ (a) and $7s$ (b), (c). Lower panel: Same for a homogeneous medium with diffusivity $A = 1$ at time steps $t = 0.7s$ (d) and $7s$ (e), (f). Note that (c) and (f) are slices taken in the x_1x_2-plane at $x_3 = 0$.*

in practice—to gain some physical intuition and start engineering and manufacturing processes of a metamaterial cloak—to analyze the coefficients defined by (2.7)–(2.8). For the reader's convenience we recall them below (only for the part $\Omega \setminus B_1$, as

coefficients inside B_1 can be arbitrary):

$$\rho_{\mathrm{cl}}(y) = \begin{cases} 1 & \text{for } y \in \Omega \setminus B_2, \\ \frac{1}{\det(D\mathcal{F}_\varepsilon)(x)}\Big|_{x=\mathcal{F}_\varepsilon^{-1}(y)} & \text{for } y \in B_2 \setminus B_1, \end{cases}$$

$$A_{\mathrm{cl}}(y) = \begin{cases} \mathrm{Id} & \text{for } y \in \Omega \setminus B_2, \\ \frac{D\mathcal{F}_\varepsilon(x) D\mathcal{F}_\varepsilon^\top(x)}{\det(D\mathcal{F}_\varepsilon)(x)}\Big|_{x=\mathcal{F}_\varepsilon^{-1}(y)} & \text{for } y \in B_2 \setminus B_1. \end{cases}$$

Remark that both the coefficients ρ_{cl} and A_{cl} depend on the regularizing parameter ε via the Lipschitz map $\mathcal{F}_\varepsilon$. In this numerical test, we plot the cloaking coefficients given in terms of the polar coordinates. Consider the Lipschitz map $\mathcal{F}_\varepsilon : \Omega \mapsto \Omega$:

$$x := (x_1, x_2) \mapsto \left(\mathcal{F}_\varepsilon^{(1)}(x), \mathcal{F}_\varepsilon^{(2)}(x)\right) =: (y_1, y_2) = y.$$

If the Cartesian coordinates (x_1, x_2) were to be expressed in terms of the polar coordinates as $(r\cos\theta, r\sin\theta)$, then the new coordinates $(\mathcal{F}_\varepsilon^{(1)}(x), \mathcal{F}_\varepsilon^{(2)}(x))$ would become $(r'\cos\theta, r'\sin\theta)$ with

$$r' := \begin{cases} r & \text{for } r \geq 2, \\ \frac{2-2\varepsilon}{2-\varepsilon} + \frac{r}{2-\varepsilon} & \text{for } \varepsilon < r < 2, \\ \frac{r}{\varepsilon} & \text{for } r \leq \varepsilon. \end{cases} \tag{5.3}$$

Bear in mind that only the radial coordinate r gets transformed by $\mathcal{F}_\varepsilon$ and the angular coordinate θ remains unchanged. Reformulating the push-forward maps in terms of the polar coordinates yields the following expressions for the cloaking coefficients in the annulus:

$$\left.\begin{aligned} A_{\mathrm{cl}}^{\mathrm{2D}} &= \mathcal{F}^* \,\mathrm{Id} = \mathtt{R}(\theta)\mathrm{diag}\left(\mathbb{A}_{11}(r'), \frac{1}{\mathbb{A}_{11}(r')}\right)[\mathtt{R}(\theta)]^\top \\ \rho_{\mathrm{cl}}^{\mathrm{2D}} &= \mathcal{F}^* 1 = \frac{r'-1}{r'}(2-\varepsilon)^2 + \frac{\varepsilon}{r'}(2-\varepsilon) \end{aligned}\right\} \quad \text{for } r' \in (1,2), \tag{5.4}$$

where $\mathbb{A}_{11}(r')$ is given by

$$\mathbb{A}_{11}(r') = \frac{r'-1}{r'} + \frac{\varepsilon}{r'(2-\varepsilon)} \qquad \text{for } r' \in [1,2] \tag{5.5}$$

and the rotation matrix

$$\mathtt{R}(\theta) = \begin{pmatrix} \cos\theta & -\sin\theta \\ \sin\theta & \cos\theta \end{pmatrix}.$$

We plot in Figure 5 the matrix entry $\mathbb{A}_{11}(r')$ given above and the push-forward density $\rho_{\mathrm{cl}}^{\mathrm{2D}}$ given in (5.4). We observe that when ε gets smaller, the radial conductivity and density take values very close to zero near the inner boundary of the cloak, which is unachievable in practice (bear in mind that the azimuthal conductivity being the inverse of the radial conductivity, the conductivity matrix becomes extremely anisotropic). Therefore, manufacturing a metamaterial cloak would require a small enough value of epsilon so that homogenization techniques could be applied to approximate the anisotropic conductivity with concentric layers of isotropic phases, as was done, e.g.,

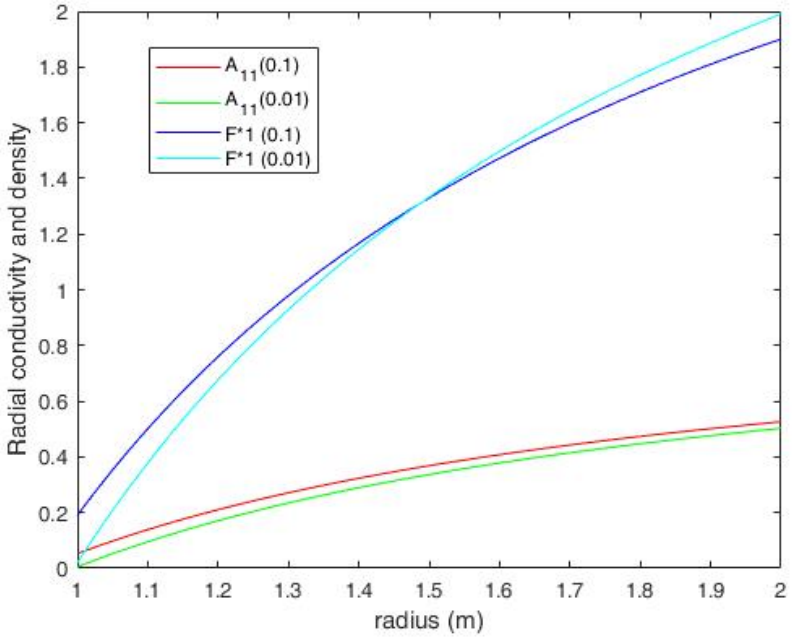

FIG. 5. *Plots of* $\rho_{\mathrm{cl}}^{2\mathrm{D}}(r')$ *and* $\mathbb{A}_{11}(r')$ *for* $r' \in [1,2]$ *and* $\varepsilon = 10^{-1}, 10^{-2}$.

for the two-dimensional metamaterial cloak manufactured at the Karlsruher Institut für Technologie [37].

In three spatial dimensions, we can recast the cloaking coefficients in the spherical coordinates (r, θ, φ). As in the cylindrical coordinate setting, only the radial variable gets modified by Kohn's transformation $\mathcal{F}^{\varepsilon}$ and the variables θ, φ remain unchanged. The transformed radial coordinate r' is given by (5.3). The push-forward maps of interest for cloaking are

(5.6)
$$\left.\begin{aligned} A_{\mathrm{cl}}^{3\mathrm{D}} &= \mathcal{F}^{*}\,\mathrm{Id} = \mathtt{R}(\theta)\mathtt{M}(\varphi)\mathrm{diag}\Big(\mathbb{B}(r'), 2-\varepsilon, 2-\varepsilon\Big)\mathtt{M}(\varphi)\,[\mathtt{R}(\theta)]^{\top} \\ \rho_{\mathrm{cl}}^{3\mathrm{D}} &= \mathcal{F}^{*}1 = \mathbb{B}(r') := (2-\varepsilon)\left(2-\varepsilon-\frac{(2-2\varepsilon)}{r'}\right)^{2} \end{aligned}\right\} \quad \text{for } r' \in (1,2)$$

with the rotation matrix $\mathtt{R}(\theta)$ in three dimensions and the matrix $\mathtt{M}(\varphi)$ given by

$$\mathtt{R}(\theta) = \begin{pmatrix} \cos\theta & -\sin\theta & 0 \\ \sin\theta & \cos\theta & 0 \\ 0 & 0 & 1 \end{pmatrix}, \quad \mathtt{M}(\varphi) = \begin{pmatrix} \sin\varphi & 0 & \cos\varphi \\ 0 & 1 & 0 \\ \cos\varphi & 0 & -\sin\varphi \end{pmatrix}.$$

Note that the matrix entry $\mathbb{B}(r')$ in the push-forward conductivity coincides with the push-forward density $\rho_{\mathrm{cl}}^{3\mathrm{D}}$. We plot in Figure 6 the radial conductivity and density in the cloaking annulus given in (5.6). One should recall that the three-dimensional spherical cloak only has a varying radial conductivity, the other two polar and azimuthal diagonal entries of the conductivity matrix being constant (i.e., independent of the radial position). Besides, the radial conductivity has the same value as the density within the cloak. All this makes the three-dimensional spherical cloak eas-

ier to approximate with homogenization techniques. However, no thermal cloak has been manufactured and experimentally characterized thus far, perhaps due to current limitations in three-dimensional manufacturing techniques; a possible route towards construction of a spherical cloak is three-dimensional printing. Similar computations in spherical coordinates, but for Pendry's singular transformation, are found in [29], where the matrix `M` was introduced to facilitate implementation of perfectly matched layers, cloaks, and other transformation-based electromagnetic media with spherical symmetry in finite element packages; see also [28], which predates the field of transformational optics.

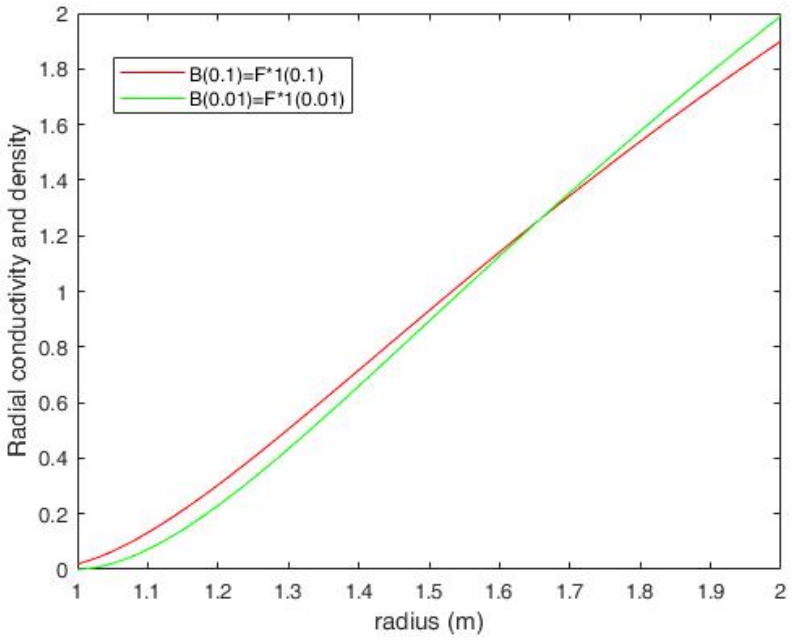

FIG. 6. *Plots of* $\rho_{\mathrm{cl}}^{\mathrm{3D}}(r') = \mathbb{B}(r')$ *for* $r' \in [1,2]$ *and* $\varepsilon = 10^{-1}, 10^{-2}$.

5.4. Spectral problems. Here we perform some numerical tests in support of the spectral result (Proposition 9) proved in this paper. The two Neumann spectral problems that we study are

$$-\Delta\phi = \mu\,\phi \quad \text{in } \Omega := (-3,3)^d, \quad \nabla\phi\cdot\mathbf{n} = 0 \quad \text{on } \partial\Omega,$$

$$-\mathrm{div}\Big(A^\varepsilon(x)\nabla\phi^\varepsilon\Big) = \mu\,\rho^\varepsilon(x)\,\phi^\varepsilon \quad \text{in } \Omega := (-3,3)^d, \quad \nabla\phi^\varepsilon\cdot\mathbf{n} = 0 \quad \text{on } \partial\Omega.$$

The coefficients are of high contrast and take the form

$$\rho^\varepsilon(x),\ A^\varepsilon(x) = \begin{cases} 1, & \mathrm{Id} & \text{for } x\in\Omega\setminus B_\varepsilon,\\ \frac{1}{\varepsilon^d}, & \frac{1}{\varepsilon^{d-2}}\mathrm{Id} & \text{for } x\in B_\varepsilon. \end{cases}$$

The first nonzero eigenvalue for the Neumann Laplacian is $\mu_2 = (\pi/6)^d$. We illustrate the result of Proposition 9 by showing that the first nonzero eigenvalue μ_2^ε for the

TABLE 1

Numerical estimate of the difference $|\ \mu_2 - \mu_2^\varepsilon\ |$ *versus the parameter* $\varepsilon = 10^{-m}$ *with* $m = 1, \ldots, 7$ *for dimension* $d = 1$*, with* $m = 1, \ldots, 3$ *for* $d = 2$*, and with* $m = 1$ *for* $d = 3$*. Same source, Neumann data, diffusivity, and density parameters as in Figure 7.*

	Numerical illustration of Proposition 9				
	dim. d	$\mu_2 = (\pi/6)^d$	μ_2^ε	$\|\ \mu_2 - \mu_2^\varepsilon\ \|$	Parameter ε
Numerical validation of $\|\ \mu_2 - \mu_2^\varepsilon\ \| \leq \varepsilon^d$	1	0.52359877559	0.5342584732	0.0106596976	$\varepsilon = 10^{-1}$
	1	0.52359877559	0.5327534635	0.0091546879	$\varepsilon = 10^{-2}$
	1	0.52359877559	0.5245077454	0.0009896980	$\varepsilon = 10^{-3}$
	1	0.52359877559	0.5236795221	0.0000807465	$\varepsilon = 10^{-4}$
	1	0.52359877559	0.5236081655	0.0000093899	$\varepsilon = 10^{-5}$
	1	0.52359877559	0.52359897453	0.0000001989	$\varepsilon = 10^{-6}$
	1	0.52359877559	0.52359888455	0.0000001089	$\varepsilon = 10^{-7}$
	2	0.27415567781	0.2741626732	0.0000069954	$\varepsilon = 10^{-1}$
	2	0.27415567781	0.2741546789	0.0000009989	$\varepsilon = 10^{-2}$
	2	0.27415567781	0.2741556795	0.0000000017	$\varepsilon = 10^{-3}$
	3	0.14354757722	0.1437347845	0.0001872072	$\varepsilon = 10^{-1}$

defect spectral problem is ε^d-close to μ_2 for various value of ε and in one, two, and three dimensions. The results are tabulated in Table 1. The associated eigenfields are also plotted in Figure 7. Note that the spectral problems in one, two, and three dimensions are solved with direct UMFPACK and PARDISO solvers using adaptive meshes with 250, 150, and 50 thousand elements, respectively. We made sure that there are at least 10^2 elements in the small defect for every spectral problem solved.

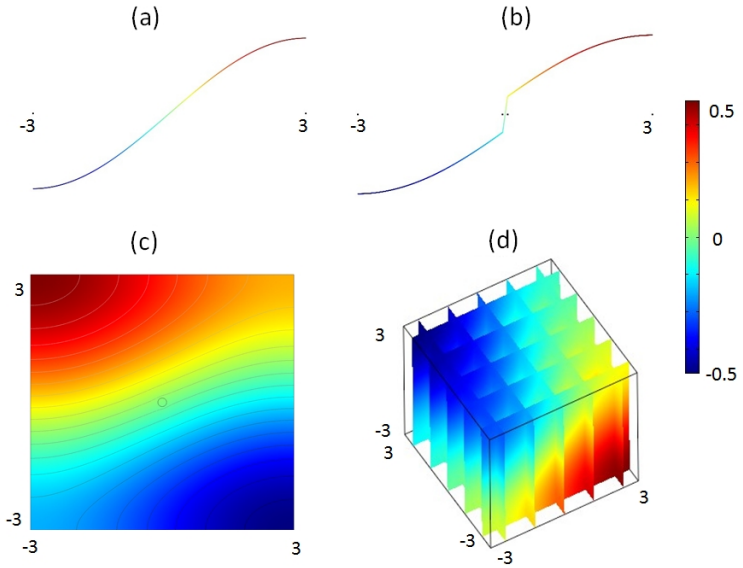

FIG. 7. *Numerical results for contour plots of eigenfields* ϕ *and* ϕ^ε *associated with* μ_2 (a) *and* μ_2^ε (b)–(d) *in one dimension* (a), (b)*, two dimensions* (c)*, and three dimensions* (d).

6. Concluding remarks. This work addressed the question of near-cloaking in the time-dependent heat conduction problem. The main inspiration is derived

from the work of Kohn et al. [22], which quantified near-cloaking in terms of certain boundary measurements. Hence the main result of this paper (see Theorem 2) asserts that the difference between the solution to the cloak problem (2.6) and that to the homogeneous problem (2.5) when measured in the $\mathrm{H}^{\frac{1}{2}}$-norm on the boundary can be made as small as one wishes by fine tuning certain regularization parameters. To the best of our knowledge, this is the first work to consider near-cloaking strategies to address the time-dependent heat conduction problem. This work supports the idea of thermal cloaking, albeit with the price of having to wait for a certain time to see the effect of cloaking. We also illustrate our theoretical results by some numerical simulations. We leave the study of fine properties of the thermal cloak problem for future investigations:

- studying the behavior of the temperature field inside the cloaked region,
- designing certain multiscale structures (à la reiterated homogenization) to achieve effective properties close to the characteristics of ρ_{cl} and A_{cl}, and
- studying thermal cloaking for time-harmonic sources.

Acknowledgments. The authors would like to thank Yves Capdeboscq for helpful discussions regarding the Calderón inverse problem and for bringing to our attention the work of Kohn et al. [22].

REFERENCES

[1] A. Alù and N. Engheta, *Achieving transparency with plasmonic and metamaterial coatings*, Phys. Rev. E (3), 72 (2005), 016623, https://doi.org/10.1103/physreve.72.016623.

[2] A. Alù and N. Engheta, *Cloaking and transparency for collections of particles with metamaterial and plasmonic covers*, Opt. Express, 15 (2007), pp. 7578–7590, https://doi.org/10.1364/oe.15.007578.

[3] H. Ammari, E. Iakovleva, H. Kang, and K. Kim, *Direct algorithms for thermal imaging of small inclusions*, Multiscale Model. Simul., 4 (2005), pp. 1116–1136, https://doi.org/10.1137/040620266.

[4] H. Ammari, H. Kang, K. Kim, and H. Lee, *Strong convergence of the solutions of the linear elasticity and uniformity of asymptotic expansions in the presence of small inclusions*, J. Differential Equations, 254 (2013), pp. 4446–4464, https://doi.org/10.1016/j.jde.2013.03.008.

[5] H. Ammari, H. Kang, and H. Lee, *Layer Potential Techniques in Spectral Analysis*, Math. Surveys Monogr. 153, American Mathematical Society, Providence, RI, 2009, https://doi.org/10.1090/surv/153.

[6] H. Ammari, H. Kang, H. Lee, and M. Lim, *Enhancement of near-cloaking. Part* II: *The Helmholtz equation*, Comm. Math. Phys., 317 (2012), pp. 485–502, https://doi.org/10.1007/s00220-012-1620-y.

[7] H. Ammari, H. Kang, H. Lee, and M. Lim, *Enhancement of near cloaking using generalized polarization tensors vanishing structures. Part* I: *The conductivity problem*, Comm. Math. Phys., 317 (2012), pp. 253–266, https://doi.org/10.1007/s00220-012-1615-8.

[8] H. Ammari and S. Moskow, *Asymptotic expansions for eigenvalues in the presence of small inhomogeneities*, Math. Methods Appl. Sci., 26 (2003), pp. 67–75, https://doi.org/10.1002/mma.343.

[9] G. Chechkin, *Homogenization of a model spectral problem for the Laplace operator in a domain with many closely located "heavy" and "intermediate heavy" concentrated masses*, J. Math. Sci., 135 (2006), pp. 3485–3521, https://doi.org/10.1007/s10958-006-0175-x.

[10] M. Chipot, *Elements of Nonlinear Analysis*, Birkhäuser Adv. Texts Basler Lehrbücher, Birkhäuser Verlag, Basel, 2000, https://doi.org/10.1007/978-3-0348-8428-0.

[11] A. Friedman and M. Vogelius, *Identification of small inhomogeneities of extreme conductivity by boundary measurements: A theorem on continuous dependence*, Arch. Rational Mech. Anal., 105 (1989), pp. 299–326, https://doi.org/10.1007/BF00281494.

[12] B. Gralak, G. Arismendi, B. Avril, A. Diatta, and S. Guenneau, *Analysis in temporal regime of dispersive invisible structures designed from transformation optics*, Phys. Rev. B, 93 (2016), 121114, https://doi.org/10.1103/physrevb.93.121114.

[13] A. Greenleaf, Y. Kurylev, M. Lassas, and G. Uhlmann, *Isotropic transformation optics: Approximate acoustic and quantum cloaking*, New J. Phys., 10 (2008), 115024, https://doi.org/10.1088/1367-2630/10/11/115024.

[14] A. Greenleaf, Y. Kurylev, M. Lassas, and G. Uhlmann, *Cloaking devices, electromagnetic wormholes, and transformation optics*, SIAM Rev., 51 (2009), pp. 3–33, https://doi.org/10.1137/080716827.

[15] A. Greenleaf, Y. Kurylev, M. Lassas, and G. Uhlmann, *Invisibility and inverse problems*, Bull. Amer. Math. Soc. (N.S.), 46 (2009), pp. 55–97, https://doi.org/10.1090/S0273-0979-08-01232-9.

[16] A. Greenleaf, M. Lassas, and G. Uhlmann, *On nonuniqueness for Calderón's inverse problem*, Math. Res. Lett., 10 (2003), pp. 685–693, https://doi.org/10.4310/mrl.2003.v10.n5.a11.

[17] D. Grieser, *Uniform bounds for eigenfunctions of the Laplacian on manifolds with boundary*, Comm. Partial Differential Equations, 27 (2002), pp. 1283–1299, https://doi.org/10.1081/pde-120005839.

[18] S. Guenneau, C. Amra, and D. Veynante, *Transformation thermodynamics: Cloaking and concentrating heat flux*, Opt. Express, 20 (2012), pp. 8207–8218, https://doi.org/10.1364/oe.20.008207.

[19] S. Guenneau and T. Puvirajesinghe, *Fick's second law transformed: One path to cloaking in mass diffusion*, J. R. Soc. Interface, 10 (2013), 20130106, https://doi.org/10.1098/rsif.2013.0106.

[20] I. Kocyigit, H. Liu, and H. Sun, *Regular scattering patterns from near-cloaking devices and their implications for invisibility cloaking*, Inverse Problems, 29 (2013), 045005, https://doi.org/10.1088/0266-5611/29/4/045005.

[21] R. Kohn, D. Onofrei, M. Vogelius, and M. Weinstein, *Cloaking via change of variables for the Helmholtz equation*, Comm. Pure Appl. Math., 63 (2010), pp. 973–1016, https://doi.org/10.1002/cpa.20326.

[22] R. Kohn, H. Shen, M. Vogelius, and M. Weinstein, *Cloaking via change of variables in electric impedance tomography*, Inverse Problems, 24 (2008), 015016, https://doi.org/10.1088/0266-5611/24/1/015016.

[23] M. Liu, Z. Mei, X. Ma, and T. Cui, *DC illusion and its experimental verification*, Appl. Phys. Lett., 101 (2012), 051905, https://doi.org/10.1063/1.4742133.

[24] H.-M. Nguyen, *Cloaking via change of variables for the Helmholtz equation in the whole space*, Comm. Pure Appl. Math., 63 (2010), pp. 1505–1524, https://doi.org/10.1002/cpa.20333.

[25] H.-M. Nguyen, *Approximate cloaking for the Helmholtz equation via transformation optics and consequences for perfect cloaking*, Comm. Pure Appl. Math., 65 (2012), pp. 155–186, https://doi.org/10.1002/cpa.20392.

[26] H.-M. Nguyen and M. Vogelius, *Full range scattering estimates and their application to cloaking*, Arch. Ration. Mech. Anal., 203 (2012), pp. 769–807, https://doi.org/10.1007/s00205-011-0459-2.

[27] H.-M. Nguyen and M. S. Vogelius, *Approximate cloaking for the full wave equation via change of variables*, SIAM J. Math. Anal., 44 (2012), pp. 1894–1924, https://doi.org/10.1137/110833154.

[28] A. Nicolet, J.-F. Remacle, B. Meys, A. Genon, and W. Legros, *Transformation methods in computational electromagnetism*, J. Appl. Phys., 75 (1994), pp. 6036–6038, https://doi.org/10.1063/1.355500.

[29] A. Nicolet, F. Zolla, Y. O. Agha, and S. Guenneau, *Geometrical transformations and equivalent materials in computational electromagnetism*, COMPEL, 27 (2008), pp. 806–819, https://doi.org/10.1108/03321640810878216.

[30] G. Pavliotis, *Stochastic Processes and Applications*, Texts Appl. Math. 60, Springer, New York, 2014, https://doi.org/10.1007/978-1-4939-1323-7.

[31] A. Pazy, *Semigroups of Linear Operators and Applications to Partial Differential Equations*, Appl. Math. Sci. 44, Springer-Verlag, New York, 1983, https://doi.org/10.1007/978-1-4612-5561-1.

[32] J. Pendry, D. Schurig, and D. Smith, *Controlling electromagnetic fields*, Science, 312 (2006), pp. 1780–1782, https://doi.org/10.1126/science.1125907.

[33] D. Petiteau, *Ingénierie de métamatériaux thermiques: Transformations d'espace et techniques d'homogénéisation appliquées à l'équation de la chaleur*, Ph.D. thesis, Aix-Marseille Université, Marseille, France, 2015, http://www.theses.fr/2015AIXM4341.

[34] D. Petiteau, S. Guenneau, M. Bellieud, M. Zerrad, and C. Amra, *Spectral effectiveness of engineered thermal cloaks in the frequency regime*, Sci. Rep., 4 (2014), 7386, https://doi.org/10.1038/srep07386.

[35] M. Raza, Y. Liu, E. Lee, and Y. Ma, *Transformation thermodynamics and heat cloaking: A review*, J. Opt., 18 (2016), 044002, https://doi.org/10.1088/2040-8978/18/4/044002.
[36] R. Schittny, M. Kadic, T. Buckmann, and M. Wegener, *Invisibility cloaking in a diffusive light scattering medium*, Science, 345 (2014), pp. 427–429, https://doi.org/10.1126/science.1254524.
[37] R. Schittny, M. Kadic, S. Guenneau, and M. Wegener, *Experiments on transformation thermodynamics: Molding the flow of heat*, Phys. Rev. Lett., 110 (2013), 195901, https://doi.org/10.1103/physrevlett.110.195901.
[38] L. Zeng and R. Song, *Controlling chloride ions diffusion in concrete*, Sci. Rep., 3 (2013), 3359, https://doi.org/10.1038/srep03359.
[39] S. Zhang, D. Genov, C. Sun, and X. Zhang, *Cloaking of matter waves*, Phys. Rev. Lett., 100 (2008), 123002, https://doi.org/10.1103/physrevlett.100.123002.